Biomedicine & Pharmacotherapy 150 (2022) 113008

Contents lists available at ScienceDirect

Biomedicine & Pharmacotherapy

journal homepage: www.elsevier.com/locate/biopha

In-silico predicting as a tool to develop plant-based biomedicines and nanoparticles: *Lycium shawii* metabolites

Afrah E. Mohammed [a], Fuad Ameen [b], Kawther Aabed [a], Rasha Saad Suliman [c,d], Sahar Saleh Alghamdi [c,d], Fatmah Ahmed Safhi [a], Dalal Sulaiman Alshaya [a], Hayat Ali Alafari [a], Areej S. Jalal [a], Areej A. Alosaimi [e], Salha Mesfer Alshamrani [f], Ishrat Rahman [g,*]

[a] Department of Biology, College of Science, Princess Nourah bint Abdulrahman University, P.O. Box 84428, Riyadh 11671, Saudi Arabia
[b] Department of Botany & Microbiology, College of Science, King Saud University, Riyadh 11451, Saudi Arabia
[c] Department of Pharmaceutical Sciences, College of Pharmacy, King Saud Bin Abdulaziz University for Health Sciences, Saudi Arabia
[d] King Abdullah International Medical Research Center (KAIMRC), Riyadh, Saudi Arabia
[e] Department of Biology, College of Science, Imam Abdulrahman Bin Faisal University, Dammam 31441, Saudi Arabia
[f] Department of Biology, College of Science, Jeddah University, Jeddah, Saudi Arabia
[g] Department of Basic Dental Sciences, College of Dentistry, Princess Nourah bint Abdulrahman University, P.O. Box 84428, Riyadh 11671, Saudi Arabia

ARTICLE INFO

Keywords:
Nanoparticles
Antibacterial
Cytotoxicity
In silico
Docking
Carbonic anhydrase IX

ABSTRACT

Introduction and purpose: In silico approach helps develop biomedicines and is useful for exploring the pharmacology of potential therapeutics using computer-simulated models. *In vitro* assays were used to determine the anti-microbial and cytotoxic efficacies of silver nanoparticles (AgNPs) synthesized with the shrub *Lycium shawii*.
Methods: In silico predicting was performed to assess the *L. shawii* metabolites identified using QTOF-LCMS for their pharmacological properties. *L. shawii* mediated AgNPs were synthesized and characterized (FTIR, TEM, SEM, DLS and EDX). The anti-bacterial efficacies of *L. shawii* extract, AgNPs, and penicillin-conjugated AgNPs (pen-AgNPs) were determined. The cytotoxicity of the AgNPs was measured against colorectal cancer cell line (HCT116), normal breast epithelium (MCF 10 A), and breast cancer cell line (MDA MB 231).
Results and discussion: Five molecules (costunolide, catechin, emodin, lyciumaside, and aloe emodin 11-O-rhamnoside) were detected in the *L. shawii* extract. AgNPs (69 nm) were spherical with crystallographic structure. All three agents prepared showed inhibitory activity against the tested bacteria, the most efficacious being pen-AgNPs. High cytotoxicity of AgNPs (IC_{50} 62 μg/ml) was observed against HCT116, IC_{50} was 78 μg/ml for MCF 10 A, and 250 μg/ml for MDA MB 231, of which cells showed apoptotic features under TEM examination. The *in silico* approach indicated that the carbonic anhydrase IX enzyme was the target molecule mediating anti-cancer and anti-bacterial activities and that emodin was the metabolite in action.
Conclusions: Combining *in vitro* studies and *in silico* molecular target prediction helps find novel therapeutic agents. Among *L. shawii* metabolites, emodin is suggested for further studies as an agent for drug development against pathogenic bacteria and cancer.

1. Introduction

In drug discovery, novel selective therapeutic agents are sought. Medicinal herbs are traditionally used to treat various pathogenic bacterial infections and cancer. The potential of these herbs as mediators in the synthesis of metal nanoparticles (NPs) has been shown by numerous studies, as reviewed recently [1–3]. Several known medical herbs, such as *Coriandrum sativum*, *Mangifera indica*, *Ocimum sanctum*, and *Bridelia retusa*, to name a few, have successfully been used to synthesize metal NPs [4–6]. Some plants, such as *Eucalyptus* sp. and *Aloe vera,* have also been used in numerous studies [7–11].

In searching for biological drugs, a useful approach would be to analyze published data on biologically active molecules present in plants. The computational *in silico* approach offers a valuable tool for searching for biological drugs. Existing information on the metabolites of an organism is searched from databases available on internet

* Corresponding author.
E-mail address: imrahman@pnu.edu.sa (I. Rahman).

https://doi.org/10.1016/j.biopha.2022.113008
Received 12 March 2022; Received in revised form 11 April 2022; Accepted 19 April 2022
Available online 27 April 2022

websites. Notably, the *in silico* approach offers the possibility of finding target compounds that inhibit disease processes, aiding in understanding the mechanism of action [12]. Moreover, *in silico* has advantages over *in vitro* experiments which are often time-consuming, require significant resources, and are vulnerable to failure. The save of time and resources is remarkable when *in silico* predictions are carried out before the compound is tested *in vitro* and *in vivo* [13]. *In vitro* tested efficacy data can also be verified using *in silico* studies [14–18]. For instance, *in silico* molecular docking studies have revealed that the inhibition of enzymes such as β-lactamase is the mechanism behind the antibacterial activity of nanomaterials [19–21]. A molecular docking study also showed the interaction of the urease enzyme with an active compound from *Hibiscus sabdariffa* (protocatechuic acid), suggesting a safe treatment option for urease-producing bacterial infections [22].

A perennial plant genus *Lycium* has traditionally been used in biomedicine. One of its species, *L. barbatum,* is well known and commonly used in many medical applications [23]. Another species, *L. chinense*, has strong anti-bacterial effects on gram-positive and gram-negative bacteria [24]. One more medicinal species, namely *L. shawii* (desert thorn or Arabian boxthorn), is a thorny shrub growing in dry areas. *L. shawii* metabolites are reported to inhibit enzymes and pathogenic bacteria [25,26], and its pharmaceutically valuable compounds have been described [27]. Based on this published information and the increasing use of safe plant metabolites in disease treatment, we chose *L. shawii* as a medicinal herb for producing silver NPs.

We aimed to find novel therapeutic agents against pathogenic bacteria and cancer using *in vitro* and *in silico* techniques. Based on previous literature we hypothesized that. *L.shawii* will be biologically active against infections. The shrub *L. shawii* was used *in vitro* to study its potential as a source of anti-microbial and anti-cancer agents, synthesizing *L. shawii*-AgNPs, of which biological activities were tested. Finally, *in silico* studies were carried out to understand the pharmacodynamics and pharmacokinetics of QTOF-LCMS identified metabolites. We have assumed that any anti-bacterial and anticancer activity of the *L. shawii* metabolites seen *in silico* is translatable to any activity of the *L.shawii* extract and *L.Shawii*-NPs observed *in vitro*.

2. Material and methods

2.1. Plant material

Lycium shawii leaves were obtained from the nursery of the royal commission for Riyadh city, Saudi Arabia. The leaves were cleaned with distilled water, oven-dried (70 °C), and ground using a milling machine (IKA-Werke, GMBH and Co., Germany). The aqueous plant extract was prepared by adding (2:100, weight: vol) to the powdered leaves and heating to 84 °C for 10 min. The suspension was filtered through Whatman Grade No. 1 filter paper, and the extract was used for NP formation and further *in vitro* studies.

For LC–QTOF-MS, *L. shawii* aqueous extract was prepared by soaking the powdered leaves in distilled water at 60 °C for 48 h. The suspension was filtered through Whatman Grade No. 1 filter paper and evaporated. One mg of the aqueous extract was dissolved in methanol (1 ml). Separation was performed using Agilent Extend-C18 column (2.1 mm × 50 mm, 1.8 μm) with the following elution gradient; 0–1 min, 5% B; 1–11 min, 5–100% B; 11–13 min,95%B; 13–15 min, 5%B; 15–16 min, 5%B using mobile phase A (0.1% HCOOH in water) and mobile phase B (0.1% HCOOH in Methanol). The injection volume was 10 μL, and the flow rate was 300 μL/min. The MS1 acquisition method was achieved in positive mode with mass ranging from 100 to 600 *m/z*. The mass spectrometer parameters were set as follows: Gas Temperature = 300 °C; Gas flow = 8 l/min; Nebulizer = 35 psig; SheathGas Temperature = 350, and SheathGas flow was 11. MS1 data was generated by Agilent Mass Hunter (Agilent Technologies) qualitative and quantitative analysis software. After conducting a mass screening on the spectrum, the chemical features were extracted from the LC-MS data using the Molecular Features Extraction (MFE) algorithm and the recursive analysis workflow.

Fourier-transform infrared spectroscopy (FTIR) test was employed to detect the possible organic components in *L.shawii* extract at the spectra between 450 and 3500 cm^{-1} by SPECTRUM100, Perkin-Elmer, Wellesley, MA, USA, utilizing a diffuse reflectance accessory [28].

2.2. AgNPs synthesis

The AgNP synthesis was carried out as described by Chandhirasekar et al. [29]. *L.shawii* extract (10 ml) was combined with $AgNO_3$ solution (90 ml, 1 mM) in a flask and kept at 80 °C for 20 min. The flask was kept at room temperature in the dark for 24 h until a stable dark color developed. After that, the mixture was centrifuged at 13000 rpm for 20 min. The pellet was washed twice with distilled water and laid on a glass plate to dry at room temperature. An AgNP solution of 1 mg/ml was prepared in distilled water for further investigations.

2.3. Penicillin-conjugated AgNPs (Pen-AgNPs) preparation

Pen-AgNPs nanocomposites were formed by adding equal concentrations of penicillin solution (1 ml, 1 mg/ml) to AgNPs solution (1 ml). The mixture was kept in the dark at RT for 48 h under shaking, centrifuged to discharge the supernatant, washed with distilled water, and centrifuged again. Finally, the pellet was placed on a glass plate to dry at RT, and 1 mg/ml was prepared for anti-bacterial examination [30].

2.4. Physicochemical characterization of AgNPs

The hydrodynamic size distribution of AgNPs was analyzed using the dynamic light scattering (DLS) technique. The size was measured with a Zetasizer (NANO ZSP, Malvern Instruments Ltd, Serial Number: MAL1118778, ver 7.11, UK) using the AgNP solution (1 ml). Using TEM, the size distribution and morphology were investigated at 80 kV voltage (JEM-1011, JEOL, Japan). Samples were prepared using a drop of colloidal solution of AgNPs on a carbon-coated copper grid (200 mesh) and dried in a vacuum desiccator [31]. A scanning electron microscope (SEM) (JEOL, JED-2200 series, Japan) supplied with energy-dispersive X-ray spectroscopy (EDX) was applied for surface analysis of NPs and to confirm the presence of Ag [32]. X-ray diffraction (XRD) analysis was performed to detect the AgNPs crystallinity using a Bruker D8 Discover instrument, Ultima IV (Cu/40 kV/40 m). The XRD scan diffraction pattern range was 20–85° with a two-theta (2θ) angle [33].

2.5. In vitro biological activities

All experiments were carried out as three replicates.

2.5.1. Anti-bacterial activity

The anti-microbial activities of the *L. shawii* extract, AgNPs, and Pen-AgNPs were determined using the agar well diffusion method. Gram-positive bacteria (methicillin-resistant *Staphylococcus aureus* (MRSA) and *S. mutans*) and gram-negative bacteria (*E. coli* and *Klebsiella pneumoniae*) were obtained from the Bio-house medical lab in Riyadh, Saudi Arabia. The strains were sub-cultured on nutrient agar medium (Oxoid) plates at 37 °C for 24 h using the direct colony suspension method, McFarland standard (0.5) bacterial suspensions (1.5×10^8 CFU/ml). Plates were inoculated with bacteria and 40 μL of the agents (AgNPs, 1 mg/ml, Pen-AgNPs, 1 mg/ml or *L.shawii* extract, 2 g/100 ml). Distilled water and penicillin (1 mg/ml) was used as the negative and positive controls, respectively. Plates were allowed to dry under sterile conditions and then incubated for 24 h at 37 °C [34]. Inhibitions areas around each well were measured in mm.

2.5.2. Anti-cancer action

A human colorectal carcinoma cell line, HCT116, was isolated from an adult male[35]. The breast cancer MDA MBA 231 was isolated from a

pleural effusion of a 51-year-old caucasian female with metastatic mammary adenocarcinoma. One normal breast epithelial cell line, MCF 10 A (ATCC-CRL-10317), was used as a negative control in the experiments [36]. Experiments were performed as reported previously 23. Cell lines were cultured in a 96-well plate at 5×10^4 cells/well in a humidified sterile incubator (air/CO_2 at 95%/5% at 37 ∘C). Media was discharged after 24 h and replaced by phenol-red free DMEM supplemented with fetal bovine serum FBS (0.5%). The cells were treated with various concentrations of AgNPs (2–4080 μg/ml) and incubated for 48 h. The media was aspirated, and the cells were washed with PBS. Cell viability was determined using the MTT assay according to the manufacturer's instructions. In brief, a volume of 20 μL of 5 mg/ml MTT reagent was added to the cells and incubated at 37 ∘C for 4 h. After the supernatant was discharged, MTT formazan was dissolved in 100 μL dimethyl sulfoxide. Cell viability was determined by measuring the absorbance at 570 nm on a Molecular Devices Spectra Max microplate reader.

2.5.3. TEM analysis for cell ultrastructural changes

MDA-MB-231 cells were cultured in 6 well plates and treated with AgNPs (250 μg/ml) for 24 h. The cells were collected, centrifuged, washed, and fixed in 4% glutaraldehyde (Product 16210, Electron Microscopy Sciences (EMS), Hatfield, PA, USA) for 2 h and in 1% osmium tetroxide (Product 19100, EMS) for 1 h. Treated cells were then dehydrated using 50%, 70%, and 100% ethanol for 10 min each. The samples were treated twice with 100% propylene oxide (Product 8.07027.1001, Merck KGaA, Darmstadt, Germany) for 15 min. Infiltration was performed using a mixture of EMbed 812 one-step single mix formula composed of 20 ml of EMbed 812 (Product 14900, EMS), 16 ml of Dodecenyl Succinic Anhydride (DDSA) (Product 13710, EMS), 8 ml of Methyl-5-Norbornene-2,3-Dicarboxylic Anhydride (NMA) (Product 19000, EMS) and 0.66–0.88 ml of 2,4,6-Tri(dimethylaminomethyl) phenol (DMP-30) (Product 13600, EMS). The samples were then soaked in a 1:1 solution of propylene oxide (embedding medium) for 1 h at room temperature, followed by a 2:1 solution of embedding medium at RT overnight. Finally, the mixture was replaced with a 100% embedding medium for 2 h at RT. Embedding was accomplished by transferring cell samples to EMS embedding capsules (Product 69910–05, EMS) and filling them with the embedding medium. The capsules were incubated in an oven at 60 °C for 24 h to make blocks. After cooling to RT, the blocks were manually trimmed. An ultra-thin section of 100–200 nm was produced using an ultramicrotome (Product PT-PC #75840, RMC Boeckeler Instruments, Inc., Tucson, AZ, USA). Sections were loaded on a grid (Product G200-Cu, EMS) and stained with 1% uranyl acetate (Product 93–2840, STREM CHEMICALS, Newburyport, MA, USA) for 15 min in the dark, rinsed 6 times with normal saline followed by 0.5% lead citrate (Product 17810, EMS) and finally rinsed with distilled water. After drying, samples were examined using a transmission electron microscope (JEOL JEM 1400, USA).

2.6. In silico prediction of the pharmacodynamics and pharmacokinetics of L. shawii metabolites

2.6.1. Prediction of anticancer activity using PASS online web server

The 2D chemical structures for each identified bioactive molecule were drawn using the Chemdraw tool and the Simplified Molecular Input Line Entry System (SMILES). The anti-cancer activity of the metabolites was predicted using the PASS Online web server (http://www.way2drug.com/passonline). A higher probability score (Pa) suggests that the compound is an active antineoplastic and anti-cancer agent [37].

2.6.2. Molecular target predictions using SWISSADME, sea search, and molinspiration

The molecular targets for the bioactive metabolites identified in *L. shawii* were predicted using SWISS Target Prediction (http://www.swisstargetprediction.ch/ [38], Sea Search (https://sea.bkslab.org/, [39] and Molinspiration (http://www.molinspiration.com/cgi-bin/properties) web servers. The SMILES for each bioactive metabolite were used as an input to generate data. Three webservers were utilized to predict the biological targets for the bioactive molecules against several targets, including GPCR ligands, ion channel modulators, kinase inhibitors, nuclear receptor ligands, protease inhibitors, and other enzymes.

2.6.3. Molecular docking of identified metabolites of human carbonic anhydrase IX enzyme using glide

The 2D chemical structures for the bioactive metabolites identified in *L. shawii* extract were prepared using the LigPrep tool in maestro molecular modeling software (Schrödinger Release 2021–4: Schrödinger, LLC, New York, NY, 2021). Several conformations were generated for each active metabolite using the ConfGen tool [40], and all structures were optimized and minimized to prepare them for docking. Moreover, the crystal structure of the human carbonic anhydrase IX (CA IX) (PDB: 5FL6, Resolution: 1.95 Å) was selected for protein preparation and grid generation using Protein Preparation Wizard [41] and Glide tools [42]. Standard precision (SP) scoring function was used, and the generated poses were subjected to post-docking analysis.

2.6.4. Molecular dynamics (MD) simulation for ligand-protein complex using desmond

The best-docked ligand-protein complex was selected for a further molecular simulation study using the Desmond tool (Schrödinger Release 2021–4: Desmond Molecular Dynamics System). The system for the ligand-protein complex was prepared using the TIP4P water (8345 molecules) model, and the system was neutralized by adding 7 Na^+. The NPT ensemble was utilized, and the complex was subjected to relaxation before the production run. The simulation run was performed for a 100 ns timescale, and the Desmond simulation interaction diagram (SID) was used for further analysis [43].

2.6.5. Pharmacokinetics of metabolites: absorption, distribution, metabolism, and excretion properties by SWISSADME webserver

The metabolites' pharmacokinetics, including absorption, distribution, metabolism, and excretion (ADME) properties, were predicted using the SWISSADME web server (http://www.swissadme.ch/) and QikProp [44] computational tools. Molecular weight, lipophilicity (Log P), solubility (Log S), blood-brain barrier (BBB) penetration, gastrointestinal (GI)/oral absorption, and violation of Lipinski's rule of five (ROF) were used as pharmaceutical parameters. Furthermore, the SWISSADME webserver was applied to predict CYP-P450 enzyme inhibition. The SMILES were used as an input, and CYP enzymes CYP1A2, CYP2C19, CYP2C9, CYP2D6, and CYP3A4 were evaluated.

2.6.6. Organ toxicity and safety predictions

ProTox-II webserver was utilized to predict the identified metabolites' organ and endpoint toxicity (hepatotoxicity, carcinogenicity, immunotoxicity, mutagenicity, and cytotoxicity). The prediction models were developed using an *in-vitro* and *in-vivo* database to ensure the prediction accuracy for molecules.

2.6.7. Statistical analysis

Two-way ANOVA was used to analyze the differences in inhibition between anti-microbial agents (*L. shawii* extract, AgNPs, Pen-AgNPs). In addition, Sidak's multiple comparisons test was performed to identify statistical differences in treatment within bacterial species. Cytotoxic data were best fitted to log (inhibitor) *vs.* response – Variable slope (four parameters) model, from which the IC_{50} was calculated. Statistical analysis was performed using GraphPad Prism Software version 9.1 (San Deigo, California, USA).

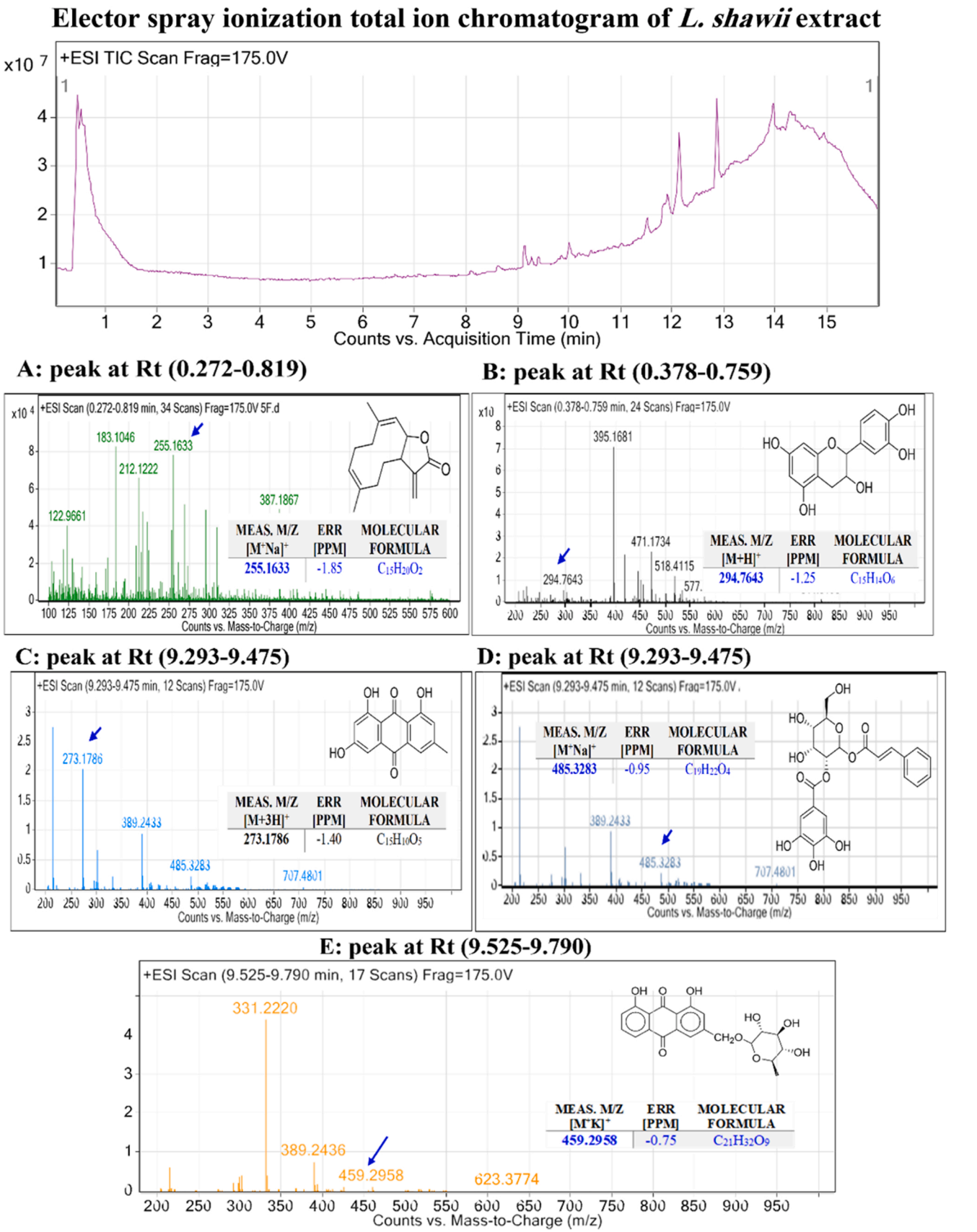

Fig. 1. Base peak chromatogram of the methanolic extract of *L. shawii* and identification of the metabolites: costunolide (A), catechin (B), emodin (C), lyciumaside (D), and aloe emodine 11-O-rhamnoside (E). Means *m/z* implies measured *m/z*.

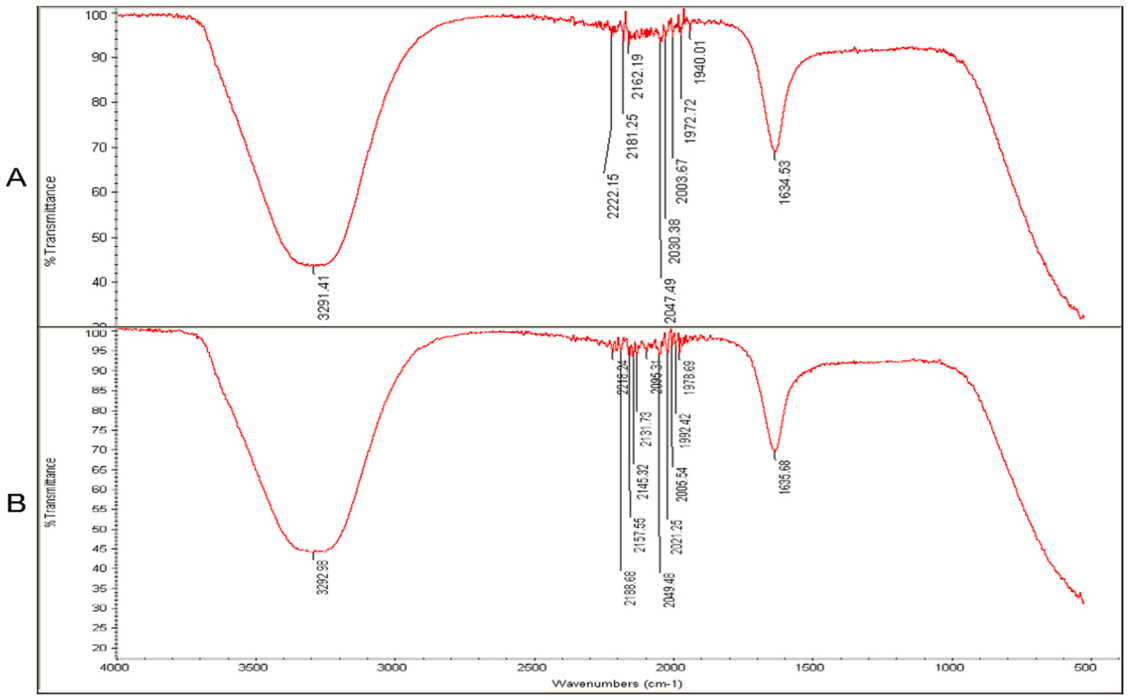

Fig. 2. FTIR data *L. shawii* extracts (A) and AgNPs mediated by *L.shawii* (B) peaks represent the functional group of expected organic compounds present.

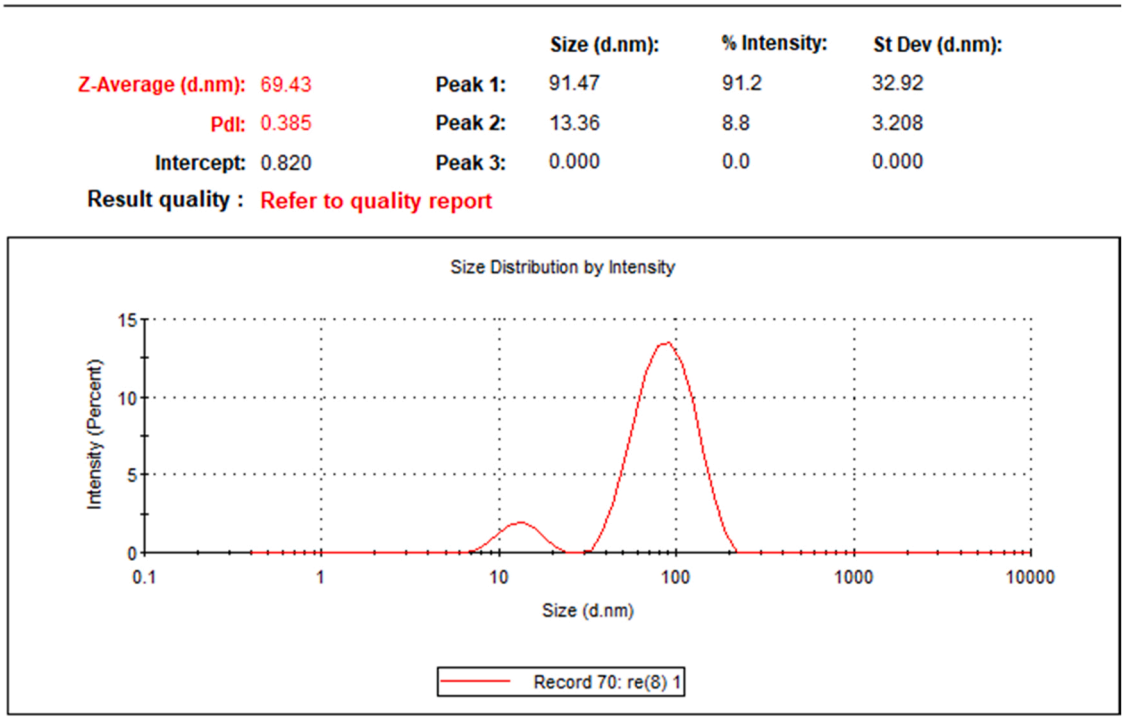

Fig. 3. Size distribution of synthesized AgNPs.

3. Results

3.1. Identification of L. shawii metabolites by LC–QTOF-MS

The electrospray ionization total ion chromatogram of *L. shawii* methanolic extract is presented in Fig. 1. After conducting a mass screening of the spectrum, the chemical features were extracted from the LC-MS by identifying the detected nodes at various retention times, with a minimum intensity of 6000 counts, which were aligned with previously detected compounds considering adducts ($[M+H]^+$, $[M+Na]^+$, $[M+K]^+$, and $[M-H]^-$). The identified compounds of *L. shawii* extract were costunolide [45], catechin [45], emodin [45], lyciumaside [46], and aloe emodine 11-O-rhamnoside [45] (Fig. 1).

Furthermore, fourier-transform infrared assessment of the *L. shawii* extract provided spectra peaks at 1634.53, 1940.01, 1972.72, 2003.67, 2030.38, 2047.49, 2162.19, 2181.25, 2222.15, and 3291.41 cm^{-1}

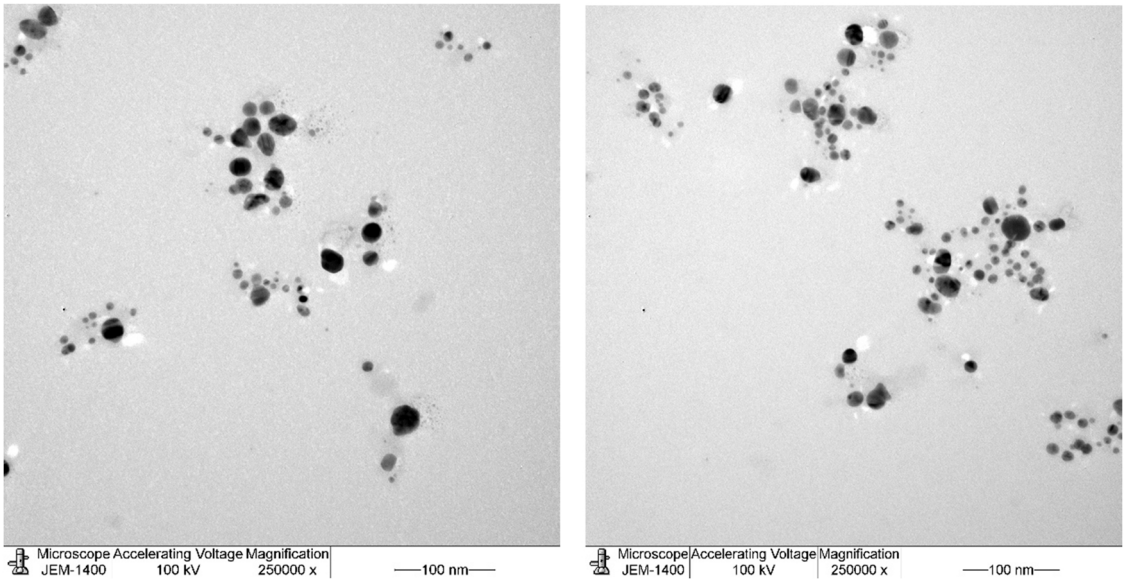

Fig. 4. TEM images showing the surface morphology and distribution of AgNPs, micrographs at scale bars: 100 nm.

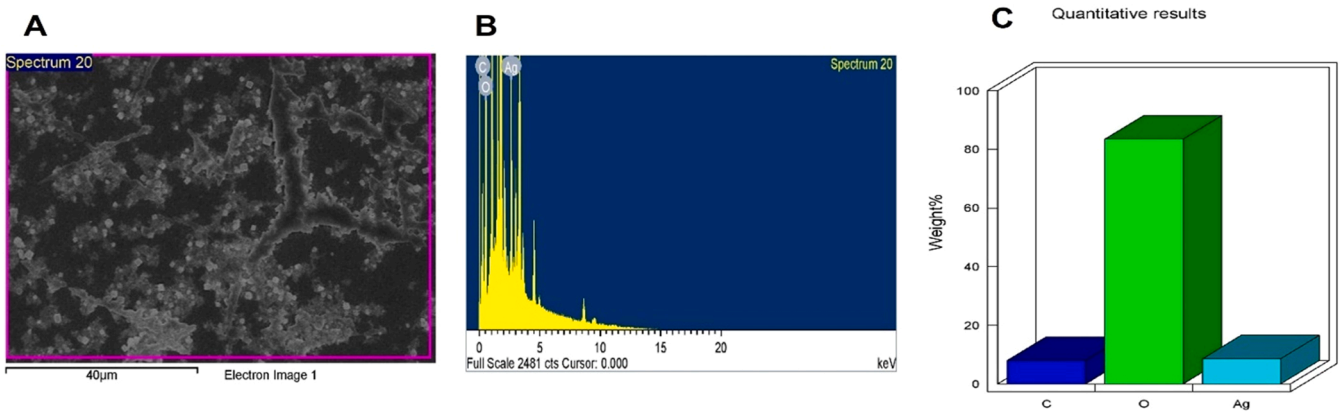

Fig. 5. (A) SEM surface morphology of AgNPs. (B and C) Quantitative data analysis of the SEM image identifying the weights of C, O, and Ag atoms using EDS.

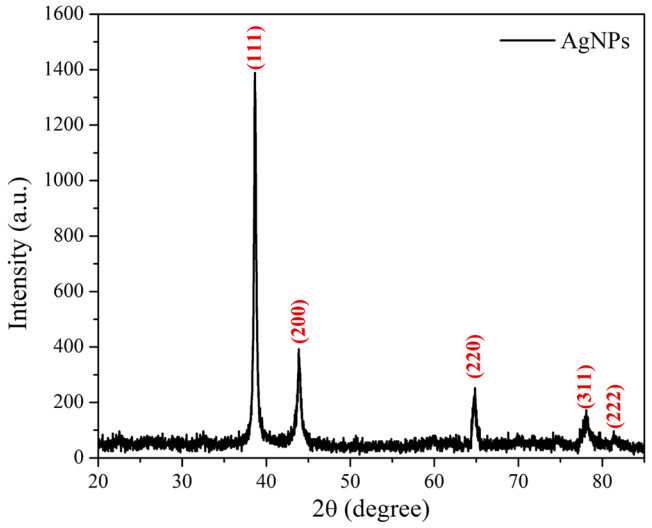

Fig. 6. XRD pattern of AgNPs indicates five intense peaks ranging from 20–85 in the whole spectrum of 2θ degrees. The intense diffraction peaks were observed at 37.4°, 43.6°, 63.9°, 77.0°, and 81.1°, corresponding to 111, 200, 220, 311, and 222 planes for fcc structure of AgNPs, respectively.

(Fig. 2A).

3.2. Characterization of AgNPs

The spectra peaks of AgNPs were at 1635.68, 1978.69, 1992.42, 2005.54, 2021.25, 2049.48, 2131.73, 2145.32, 2157.55, 2188.68 and 3292.98 cm^{-1} (Fig. 2B). A slight difference in the magnitude of the absorption bands was observed between the AgNPs and plant extract. DSL data identified AgNPs to have an average size of 69.43 nm diameter (Fig. 3). TEM images revealed spherical and well dispersed nanosize AgNPs (Fig. 4). EDX spectroscopy attached with an SEM microscope is too used to recognize the elemental configuration of the biosynthesized AgNPs. The observed EDX spectrum of AgNPs is well represented in Fig. 5, which shows the confirmation of silver (Ag), oxygen (O), and carbon (C) at their corresponding energy value. The diffraction peaks for XRD analysis were at 37.4°, 43.6°, 63.9°, 77.0°, and 81.1° correlating with the following planes: 111, 200, 220, 311, and 222, respectively, as presented in Fig. 6. Results were in agreement with the values for a face-centered cubic (fcc) structure of Ag which confirmed the synthesis of AgNPs.

3.3. Anti-bacterial activity

Tested bacteria showed sensitivity to both AgNPs and Pen-AgNPs,

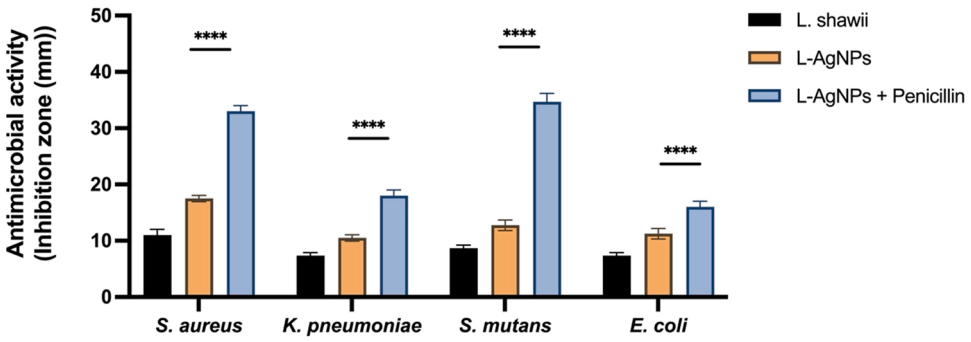

Fig. 7. Anti-bacterial activity as inhibition zones of *L. shawii* extract (*L. shawii*), AgNPs (L-AgNPs) and Pen- AgNPs (L-AgNPs + penicillin). * ** * refers to a significant difference between anti-microbial agents (two-way ANOVA, $p < 0.0001$).

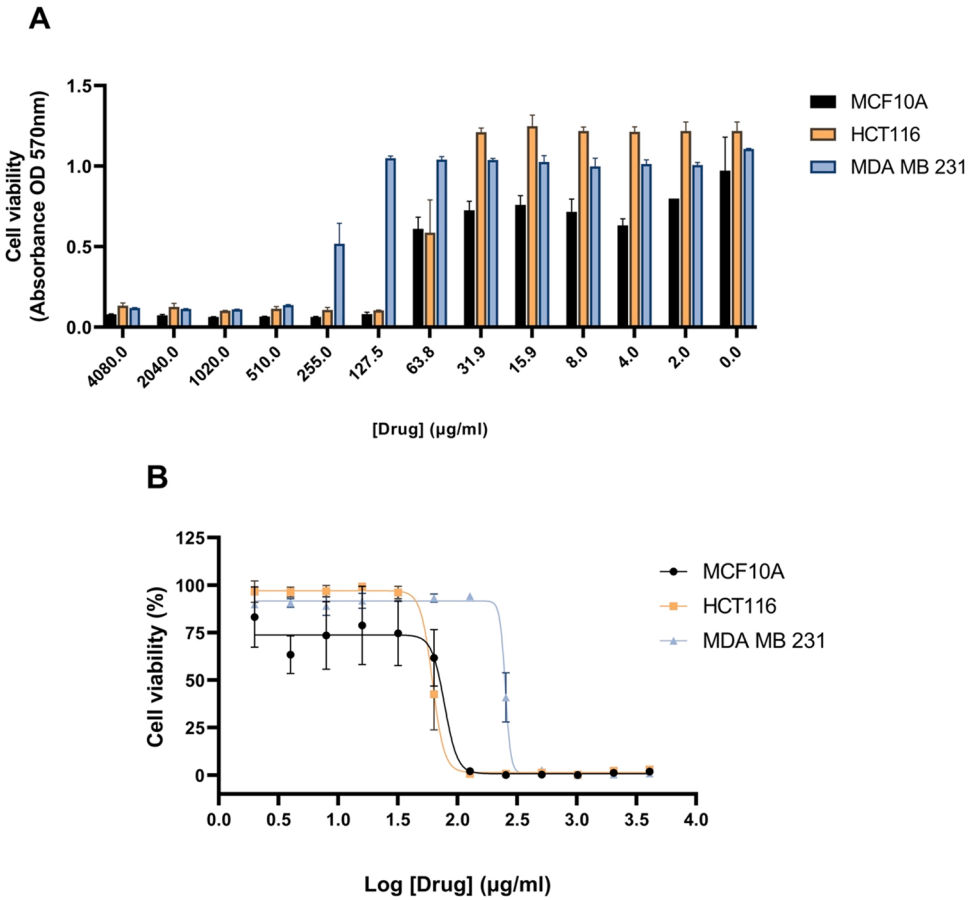

Fig. 8. (A) Cytotoxic effect of various concentrations of AgNPs on cancer cells; HCT116 and MDA MB 231 and control MCF 10 A. (B) Normalized cytotoxic response plotted as log dose AgNPs against % cell viability of cancer cell lines; HCT116 and MDA MB 231 and control MCF 10 A.

but the zone of inhibition was significantly greater for the latter ($p < 0.0001$) (Fig. 7). The inhibition zone of AgNPs for gram-positive *S. aureus* was 17.50 ± 0.57 mm and for *S. mutans* 12.75 ± 0.96 mm, while for gram-negative *K. pneumonia,* it was 10.50 ± 0.58 mm and for *E. coli* 11.25 ± 0.96 mm. For Pen-AgNPs, the anti-bacterial activity was greater against gram-positive than gram-negative bacteria. The inhibition zones were, for *S. aureus* 33.00 ± 1.00 mm, *S. mutans* 34.67 ± 1.53 mm, *K. pneumonia* 18.00 ± 1.00 mm, and *E. coli* 16.00 ± 1.00 mm ($p < 0.0001$). The *L. shawii* extract inhibited all tested bacteria but significantly less than the AgNPs and Pen-AgNPs. The zones of inhibition were for *S. aureus* 11.00 ± 1.00 mm, *S. mutans* 8.66 ± 0.58 mm, *K. pneumonia* 7.33 ± 0.58 mm, and *E. coli* 7.33 ± 0.58 mm (Fig. 6). A significant difference in the effects of the treatments was observed for all tested bacteria ($p < 0.0001$). Additionally, a considerable difference in the interactions between bacteria for any one of the treatments was also observed ($p < 0.0001$).

3.4. Cytotoxicity

A dose-dependent sigmoidal inhibitory response was observed, causing a reduction in cell viability ($p < 0.0001$) for all three tested cell lines (human cancer cell lines; HCT116 and MDA MB 231 and one normal cell line; MCF 10 A) (Fig. 8A). Each data set was best fitted to the model log (inhibitor) *vs.* response – Variable slope (four parameters) ($p < 0.0001$). IC_{50} values were 77.87 µg/ml for the normal cell line, MCF10A, 61.74 µg/ml, and 251.80 µg/ml, respectively, for the two

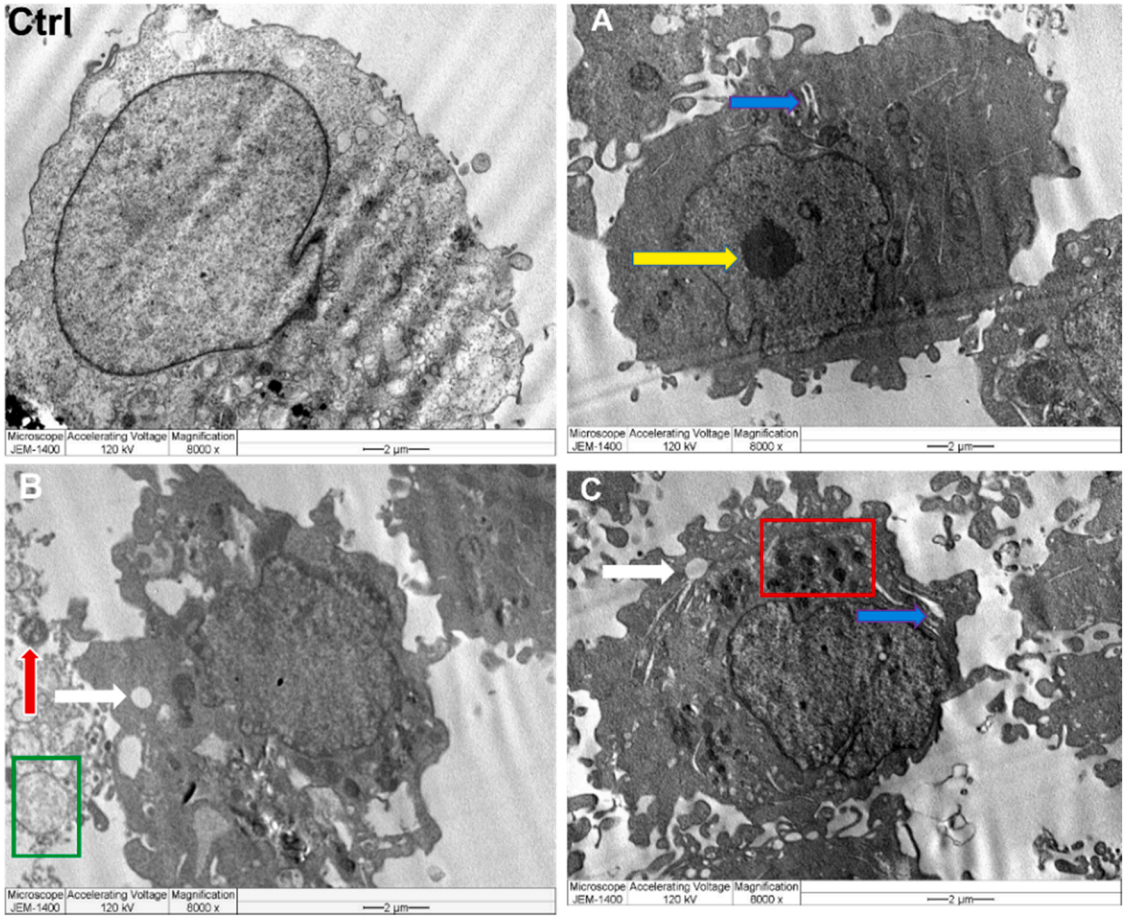

Fig. 9. : TEM images of MDA MB 231 cell lines, Ctrl refers to the control displaying cell shape and comprehensive nucleus and organelles at × 8.000 magnification, bar 2 µm. A B and C are the cells treated with the same concentration of AgNPs at the same magnification but in three different fields of view. Ultrastructural changes display apoptosis characteristics such as irregular cell shape besides peroxisomes (red square), enlarged mitochondria (green square), damaged mitochondria (red arrow), condensed nucleolus (yellow arrow), lipid droplet (white arrow), and enlarged vacuoles (blue arrow).

Table 1
Anti-cancer activity scores of *L. shawii* metabolites according to PASS Online Webserver.

Anticarcinogenic Activity	Probability of being Active (Pa)	Probability of being Inactive (Pi)
Costunolide	0.950	0.004
Catechin	0.795	0.005
Emodin	0.791	0.013
Lyciumaside	0.878	0.003
Aloe emodine 11-O-rhamnoside	0.818	0.005

cancer cell lines HCT116 and MDA MB 231 (Fig. 8B).

3.5. TEM analysis of AgNPs treated cancer cells

The morphology of AgNPs-treated MDA MB 231 cells was distinctly altered compared to untreated MDA MB 231 cells. The cells appeared to have membrane blebbing, appearing leaky and cellular debris was found scattered around the cell. Ultrastructural changes were observed. Apoptosis was observed as irregular nuclei and cell shapes besides peroxisomes, enlarged mitochondria, damaged mitochondria, condensed nucleolus, lipid droplet, and enlarged vacuoles (Fig. 9).

3.6. In silico prediction of the pharmacodynamics and pharmacokinetics of L. shawii extract metabolites

3.6.1. Anti-cancer activity

Costunolide exhibited the highest probability score as an anticarcinogenic agent, followed by Lyciumaside, Aloe emodine 11-O-rhamnoside, catechin, and Emodin (Table 1).

3.6.2. Molecular target predictions

Three web servers predicted biological targets for the identified metabolites (Table 2). The five identified *L. shawii* metabolites showed a high probability as enzyme inhibitors. SWISS Target Predictions and Sea Search suggested carbonic anhydrase (CA) IX enzyme as a potential biological target (Summarized in Table 2, Fig. 10). As an enzyme inhibitor, costunolide exhibited the highest probability score, followed by catechin, aloe emodine 11-O-rhamnoside, lyciumaside, and emodin.

3.6.3. Molecular docking of CA IX enzyme

The docking protocol was validated by a one-step redocking of the native ligand Y0R into the CA IX crystal structure. The generated docked poses demonstrated a similar binding mode and interactions as the native crystal structure. The five docked *L. shawii* metabolites formed several interactions, including Zn coordination and hydrogen bond interactions with multiple amino acid residues (except costunolide) (Table 3), the detailed 2D molecular interaction for the identified metabolities are summarized in Fig. S1. Emodin demonstrated the best docking score (−5.732) among the docked compounds with similar Zn

Table 2
Biological targets and probability score of *L. shawii* metabolites according to SWISS Target Prediction, Sea Search, and Molinspiration web server.

L. shawii metabolite	Target Predictions		
	SWISS Target Prediction	SEA Search	Molinspiration
Costunolide	Carbonic anhydrase	Prostaglandin G/H synthase 2	GPCR ligand 0.24 Ion channel modulator 0.07 Kinase inhibitor − 0.52 Nuclear receptor ligand 0.96 Protease inhibitor − 0.28 Enzyme inhibitor 0.77
Catechin	No similar actives found.	Carbonic anhydrase	GPCR ligand 0.41 Ion channel modulator 0.14 Kinase inhibitor 0.09 Nuclear receptor ligand 0.60 Protease inhibitor 0.26 Enzyme inhibitor 0.47
Emodin	Estrogen receptor	Estrogen receptor	GPCR ligand − 0.14 Ion channel modulator − 0.14 Kinase inhibitor 0.07 Nuclear receptor ligand 0.17 Protease inhibitor − 0.21 Enzyme inhibitor 0.21
Lyciumaside	Carbonic anhydrase	Carbonic anhydrase	GPCR ligand 0.03 Ion channel modulator − 0.12 Kinase inhibitor − 0.16 Nuclear receptor ligand 0.02 Protease inhibitor 0.02 Enzyme inhibitor 0.27
Aloe emodine 11-O-rhamnoside	Carbonic anhydrase	DNA topoisomerase	GPCR ligand 0.12 Ion channel modulator 0.07 Kinase inhibitor 0.06 Nuclear receptor ligand 0.07 Protease inhibitor 0.27 Enzyme inhibitor 0.45

coordination interaction relative to the native ligand. Emodin exhibited hydrogen bond and pi-pi interactions with HIS94 and THR200 residues. Moreover, the Zn coordination and binding mode were comparable to the native ligand in the CA IX crystal structure (Fig. 11**)**. The 2D chemical structure and interactions of the Identified *Lycium shawii* Metabolites with Carbonic Anhydrase (CA) IX enzyme using Glide software (Supplementry.

3.6.4. Molecular dynamic simulation of L. Shawii metabolites into the crystal structure of CA IX enzyme

The root means standard deviation graph for the simulated complex indicated that the docked pose was stable during the simulation time due to less than 3.00 Å fluctuation in RMSD values over 100 ns (Fig. 12, A). Moreover, the protein-ligand contacts with the amino acid residues were stable during the simulation. The contacts included HIS94 (100% of simulation time), HIS96 (90% of simulation time), GLU106 (90% of simulation time), HIS119 (90% of simulation time), and THR201 (90% of simulation time) (Fig. 12, B). In addition, the Zn coordination between O in emodin and Zn was maintained during 100 ns, indicating the coordination's stability (Fig. 12, C).

3.6.5. Predictions of ADME properties

The molecular weights of the five *L. shawii* metabolites were below 500 DA. Costunolide had the highest lipophilicity (Table 4**,** Fig. 13) with an acceptable degree of solubility that allowed the molecule to be permeable to cross the blood-brain barrier while demonstrating high gastrointestinal (oral) absorption. Catechin and emodin exhibited a similar profile in which both compounds possessed moderate lipophilicity and solubility with high gastrointestinal absorption and no blood-brain barrier penetration. Furthermore, Lyciumaside and Aloe-emodin 11-O-rhamnoside showed the lowest lipophilicity and good solubility with low gastrointestinal absorption and no crossing to the blood-brain barrier. Lyciumaside was the only metabolite that violated Lipinski's five hydrogen bond donor and acceptor rules.

3.6.6. Cytochromes (CYP) P450 enzymes inhibition profile

Catechin, Lyciumaside, and Aloe emodine 11-O-rhamnoside did not possess any inhibition on CYP enzymes (Table 5), suggesting a safe profile for these active compounds. However, Costunolide demonstrated inhibition on CYP2C19 and CYP2C9, while emodin exhibited CYP1A2 and CYP3A4 enzyme inhibition that could potentially affect drugs metabolized by these enzymes.

3.6.7. Organ toxicity predictions

ProTox-II web server showed no organ or endpoint toxicity of any type for catechin (Table 6, and Fig. 14). On the contrary, Costunolide, Lyciumaside, and Aloe emodine 11-O-rhamnoside demonstrated a potential immunotoxicity. Only Emodin and Aloe emodine 11-O-rhamnoside exhibited potential mutagenicity. Catechin was an inactive toxin suggesting the safest profile among the *L. shawii* metabolites.

4. Discussion

4.1. L. shawii metabolites

The secondary metabolites identified from *L.shawii* extract have previously been recognized for their antioxidant and cytotoxic capabilities. Costonulide is a naturally occurring sesquiterpene lactone found in many edible plants such as lettuce [47]. Recently, it was shown to have anti-cancer activity against triple-negative breast cancer cell line MDA MB 231 [45]. Catechin is a flavonoid found in numerous edible plants and green tea. It has antioxidant, anti-inflammatory, and anti-cancerous properties [48]. Lyciumaside is a diacylglyceride initially identified from *L. shawii* and described as a robust antioxidant [46]. Emodin belonging to anthraquinones, is found in rhubarb and is well known for its anti-inflammatory, antioxidant, and anti-cancer activity [49]. In addition, its anti-microbial property increases the permeability of bacterial membranes and prevents normal cellular functions due to interactions with essential functional proteins [50]. However, emodin has poor oral bioavailability, and high doses can cause renal and hepatic toxicity [49]. Aloe-emodin is an isomer of emodin found in aloe latex with similar therapeutic properties to emodin. Both have been shown to suppress breast cancer cell proliferation by suppressing ER-α transcription, but aloe-emodin promotes ER- α ubiquitination [51]. Interestingly, aloe-emodin has antioxidant effects at low concentrations but is pro-oxidant at high concentrations [52].

The compounds have been reported in the literature to have

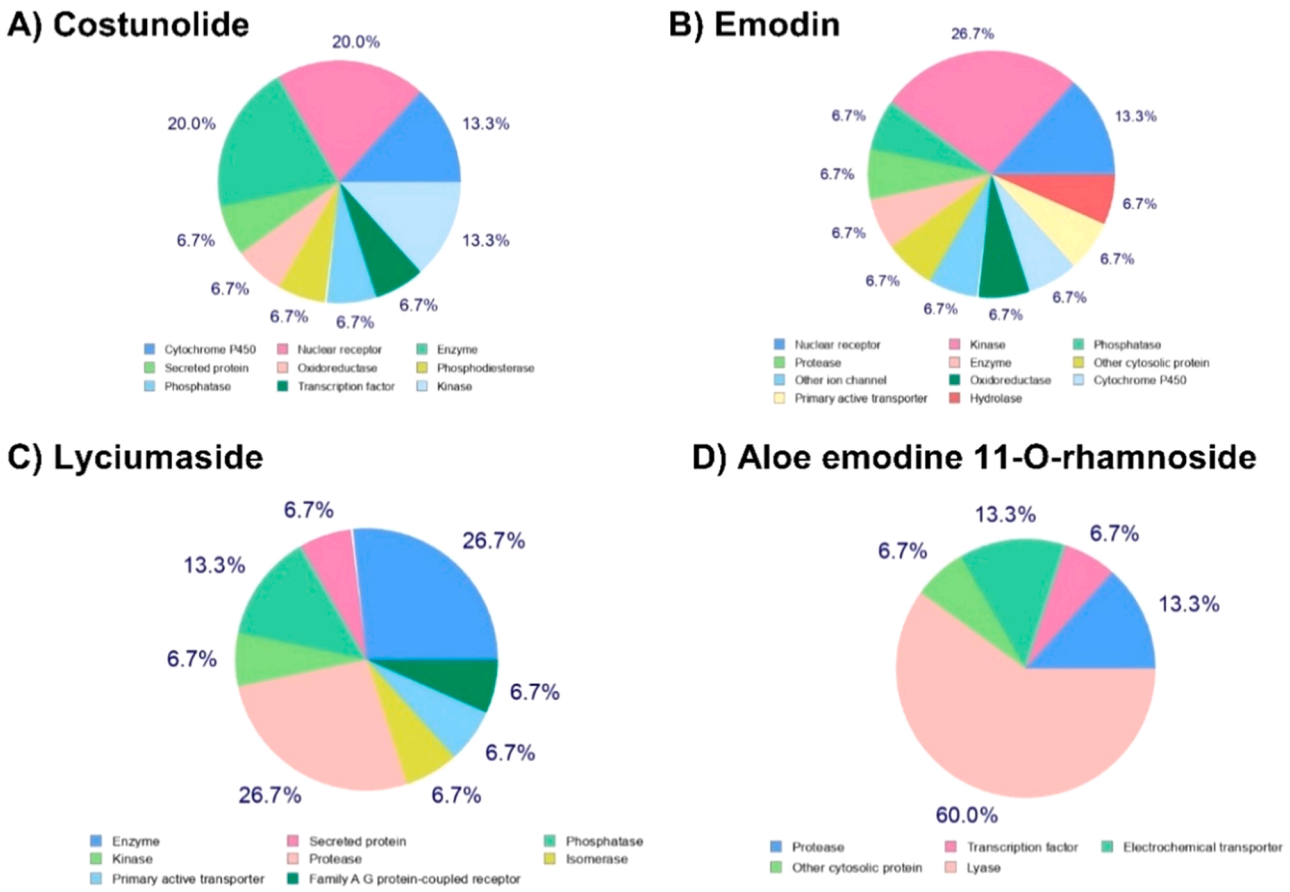

Fig. 10. The Predicted Molecular Targets (%) for L. shawii identified Metabolites using SWISS ADME Webserver. No targets were found for catechin.

Table 3
The SP docking Scores for the Identified *L. shawii* Metabolites with Carbonic Anhydrase IX enzyme using Glide.

Compound Name	Standard-Precision (SP) Glide Score	Interactions with amino acid residues
Costunolide	-4.185	No interaction
Catechin	-5.419	HIS94, PRO202, and ZN1260
Emodin	-5.732	HIS94, THR200, and ZN1260
Lyciumaside	-4.513	PRO202, THR200, and ZN1260
Aloe emodine 11-O-rhamnoside	-4.280	ASP131, THR201, and ZN1260

cytotoxic potential. Emodin, aloe emodin-11-O-rhamnoside, and lyciumaside showed weaker antiproliferative potential in the triple-negative breast cancer cell line (MDA-MB-231 IC_{50}>72 μM) than aloe emodin (31 μM) [45]. Costunolide was a more potent antioxidant than emodin, aloe emodin-11-O-rhamnoside, and lyciumaside (42 μM) [45]. However, catechin was the most potent antioxidant tested (IC_{50} =55 μM) [45]. Previous *in silico* studies predicted costunolide to exert its anti-cancer effects strongly *via* the carbonic hydrase II enzyme [45].

4.2. AgNPs synthesis

FTIR analysis identified proteins and polyphenolics in the original *L. shawii* extract and AgNPs; however, a shift in peaks was noted, indicating their role as reducing and stabilizing mediators in the fabrication process. Peaks detected at a range near 3300 cm^{-1} could be linked to OH groups of polyphenolic and N-H stretching of amines [53]. Furthermore, peaks for amide 1 and carbonyl (C = O) stretching of proteins were noted at 635.68 for the *L.shawii* extract and AgNPs [53,54]. After mixing the $AgNO_3$ and *L.shawii* extract, a change of the solution to a dark brown color indicated the successful synthesis of AgNPs, which were spherical and well distributed at mean sizes of nano-range. Furthermore, the EDX spectrum of AgNPs is similar to that previously reported [55], rather than observing a slightly spiked carbon peak. The O and C peaks confirmed the presence of carbon-based stabilizers in the sample, suggesting utilization of the phytochemicals in NP formation. Moreover, the presence of element C may correspond to the carbon type utilized to mount the desired sample during the experiment, and the presence of element O may refer to the surface oxidation [56]. The recorded XRD data indicated crystallographic structure and diffraction planes that belonged to the fcc structure of AgNPs.

One study formed AgNPs using the fruit extract *L. chinense,* which provided NPs with an average size of 20–50 nm[57]. Another study obtained even smaller AgNPs using the aqueous extract of *L. barbarum* [58]. A wide range of AgNPs sizes obtained from the same plant genus highlights the variations within species-dependent metabolites and their significant role in the reduction process of forming AgNPs.

4.3. Anti-microbial activity of L. shawii and AgNPs

We can verify our hypothesis with the observations of the anti-bacterial activity of *L. shawii* extract and *L. shawii*-AgNPs. The current study revealed the anti-microbial activity of *L. shawii,* AgNPs, and pen-AgNP. The *L. shawii* extract had less antimicrobial activity than the AgNPs. The conjugated Pen-AgNPs boasted additional anti-microbial properties, and it was more effective on the gram-positive bacteria than the gram-negative bacteria. According to our findings, conjugation with penicillin confers a synergistic anti-microbial effect, more profound

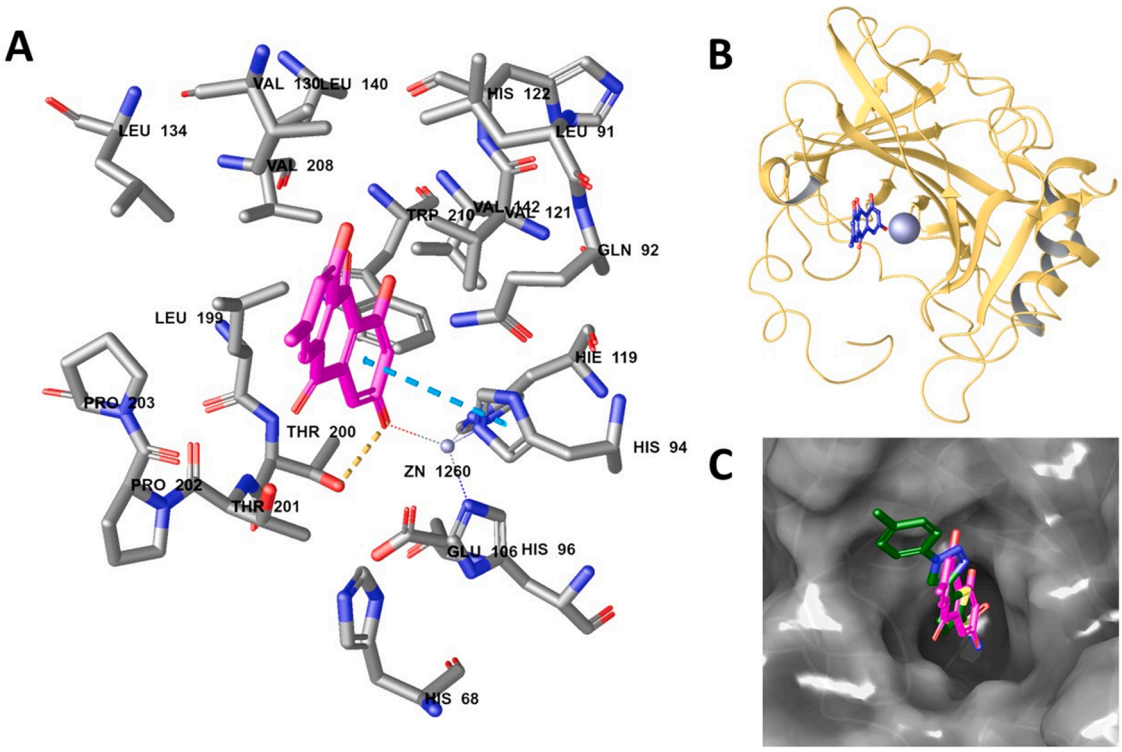

Fig. 11. (A) Molecular interactions of CA IX enzyme with emodin, (B) CA IX containing Zn with emodin, (C) Overlay of the binding mode of the native ligand Y0R with emodin within a binding site of CA IX.

in gram-positive bacteria. The antimicrobial effect may be further increased by using bimetallic NPs, as shown previously [59,60]. It is essential to identify if the activity observed in the current study can be broadly applied. Thus the AgNPs and the pen-AgNPs should be screened on a larger panel of gram-positive and gram-negative bacteria. The present findings agree with the many reports that showed enhanced additive or synergistic effects of conjugated antibiotic forms of either gold or silver nanoparticles [61–63]. The conjugated material was uniform, well distributed, and not clumped together, which allowed easy entry and penetration into the cell wall, especially in the case of the gram-positive bacteria allowing the synergistic effect to be observed. Indeed, no or minor anti-microbial effects were seen in instances where conjugation had caused aggregation and compromised the nano-particulate structure [35].

4.4. Cytotoxic effect of AgNPs

The cytotoxic and antioxidant effects of natural plant products are diverse when comparing different neoplastic cells and normal cells. Cytotoxicity of the synthesized AgNPs was measured against one normal breast epithelial cell line (MCF 10-A), one breast cancer cell line (MDA MBA 231), and one colorectal cancer cell line (HCT116). Both these cancer lines are known to be highly aggressive. AgNPs were cytotoxic on all tested cell lines, including the normal cell line. The most potent cytotoxic effect was observed in the colorectal cancer cell line (62 μg/ml AgNPs), which displayed a 4-fold greater potency than the breast cancer cell line (252 μg/ml AgNPs). In addition, a relatively potent cytotoxic effect was also observed in the control breast epithelial cell line (77.87 μg/ml AgNPs). Although the AgNPs were more potent in the control cell line than in the breast cancer cell line, it was less efficacious in the control cell line, indicated by a higher proportion of normal cells remaining viable, denoted by the smaller span of the curve. Therefore we can conclude that there appears to be little therapeutic potential of the AgNPs in the case of metastatic mammary adenocarcinoma but it may be useful in colorectal cancer. However, the AgNPs must be tested against a larger panel of normal and cancerous cell lines to accurately identify its potential use and selectivity in treating neoplasms . We believe the current study to be the first to prepare AgNPs using *L. shawii*. Previous studies highlight the broad cytotxicity profile of the *Lycium* species. *L. barbarum*-AgNPs displayed negligible cytotoxic effects on mouse embryonic cell lines [58]. *L. chinese*-AgNPs displayed strong cytotoxic properties against a breast cancer cell line (MCF7) and lower toxicity against normal murine macrophage cells (RAW264.7) [57]. Different species of *Lycium* have diverse abilities to form AgNPs, and their cytotoxic profiles vary due to the presence of secondary metabolites. For example, *L. barbarm* extract was cytotoxic against a selection of cancer cell lines to various degrees [64]. The *L. schweinfurthii* extract contains flavonoids that mediated cytotoxic effects on colon and skin cancer cells, while minimal cytotoxicity was observed against normal cell lines [30]. A recent study on *L. shawii* identified several compounds, mainly flavonoids, and phenolics, responsible for mediating cytotoxic and anti-bacterial effects [25]. Based on the current data, we conclude that *L. shawii*-AgNPs have therapeutic potential, but since very few studies have explored the safety profile based on the selectivity to cancerous *vs.* normal tissue, carefully designed experiments are required to elucidate the potential therapeutic use in humans.

4.5. In Silico pharmacodynamic and pharmacokinetic analysis of *L. shawii* metabolites

In the present study, we sought to utilize computational approaches to provide additional molecular insights to our experimental findings for the identified metabolites in the *L. shawii* extract, which could be good reducing agents in the fabrication of AgNPs. The PASS online web server's predicted activity revealed high anti-cancer properties for the five identified metabolites. Furthermore, the molecular targets prediction study suggested that the Carbonic Anhydrase enzyme could be a potential target for mediating the anti-cancer [65–68] and antibacterial activities [68,69] since most of the identified metabolites showed a high probability at this target. The Carbonic Anhydrase IX enzyme selection

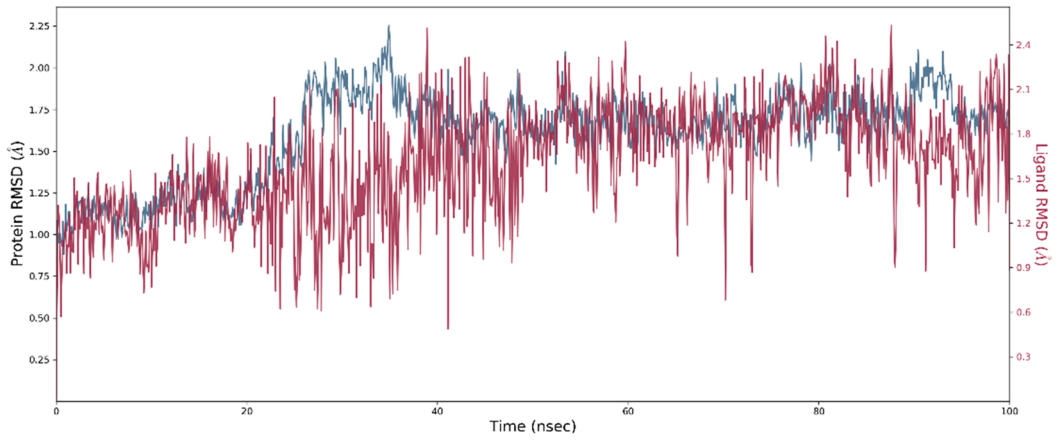

A) RMSD graph for the ligand-protein complex for 100 ns.

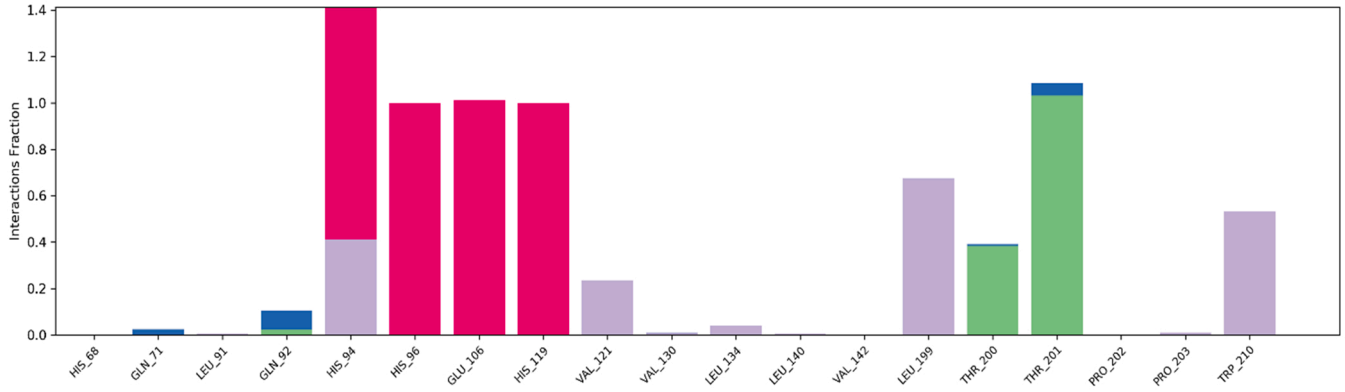

B) Protein-ligand contacts for 100 ns. Green (H-bonds), Purple (hydrophobic), Red (ionic), and blue (water bridge).

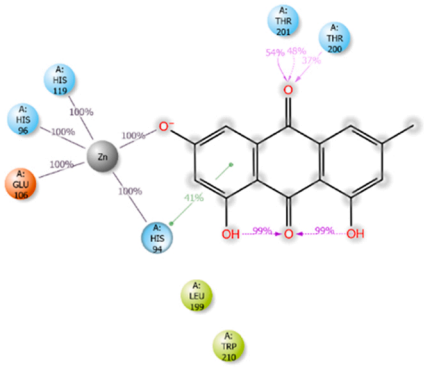

C) Ligand atom's interactions with CA IX residues for 100 ns. Hydrogen bonds (purple), green (hydrophobic), grey (metal coordination).

Fig. 12. Detailed Protein-Ligand Interactions during the Simulation Time (100 ns) for Emodin-Carbonic Anhydrase IX complex.

was based on the reported studies that showed increased expression levels in HCT116 and MDA-MB-231 cancer cells [70–73], suggesting inhibition of CA IX could be a novel therapeutic approach for an invasive type of cancer. Moreover, it has been reported that CA IX inhibitors possess anti-cancer and antibacterial activities [74,75], indicating dual therapeutic action for treating fatal human diseases.

In vitro, experimental testing of the *L. shawii* extract exhibited promising anticancer and antibacterial activity, which may result from inhibition of the CA IX enzyme, as was reported in a previous study that demonstrated similar biological activities mediated *via* CA IX [68]. To

Table 4
Predicted values for ADME Properties and pharmacokinetics for the Bioactive Molecules Identified in *L. shawii* extract using SWISSADME and QikProp Tools.

Compound Name	Molecular Weight		Log Po/w		Log S		Blood-brain barrier Permeant		GI Absorption		Rule of Five
	SWISS ADME	QikProp	SWISS ADME	QikProp	SWISS ADME	QikProp	SWISS ADME	QikProp	SWISS ADME	QikProp	SWISSADME
Costunolide	232.32	232.322	3.55	2.748	-3.05 Soluble	-3.1	Yes	1	High	100	Yes; 0 violation
Catechin	290.27	290.272	1.22	0.444	-2.14 Soluble	-2.502	No	-2	High	61.245	Yes; 0 violation
Emodin	270.24	270.241	1.89	1.234	-3.91 Soluble	-2.995	No	-2	High	68.565	Yes; 0 violation
Lyciumaside	462.40	462.409	-0.08	-0.22	-1.18 Soluble	-3.017	No	-2	Low	17.588	No; 2 violations: NorO> 10, NHorOH> 5
Aloe emodine 11-O-rhamnoside	416.38	416.384	0.07	-0.051	-2.79 Soluble	-3.17	No	-2	Low	51.04	Yes; 0 violation

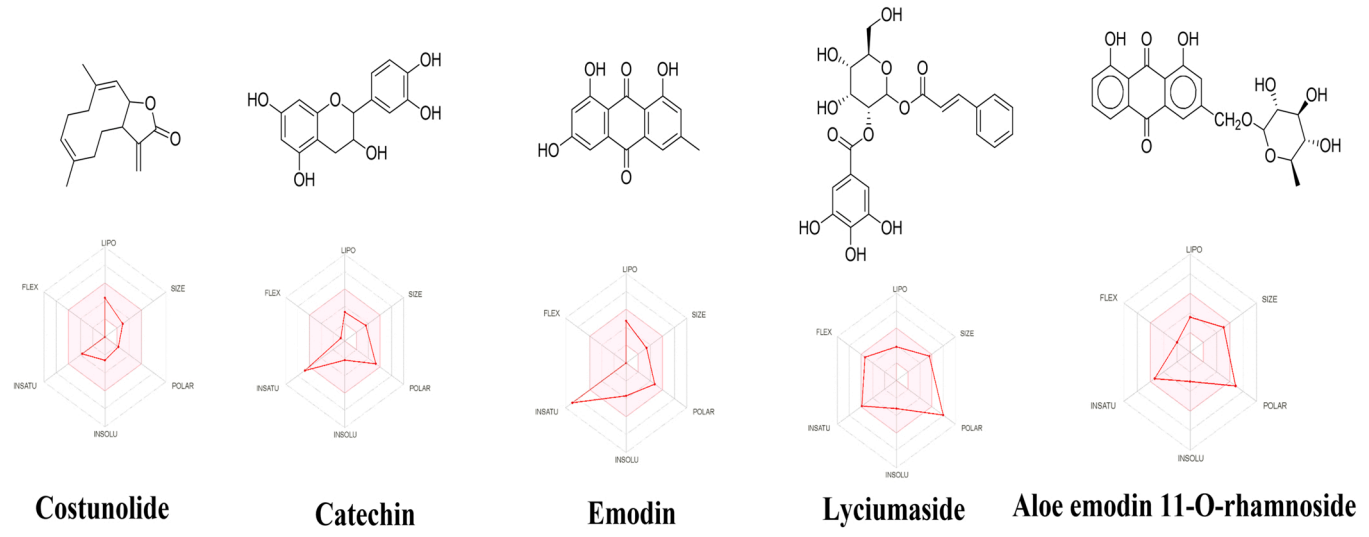

Fig. 13. ADME Properties for the *L. shawii* Metabolites using SWISSADME Webserver. LIPO: Lipophilicity, Size: Molecular weight, POLAR: solubility, INSOLU: insolubility, INSATU: insaturation, and FLEX: flexibility. The properties involved in the colored zone are preferred for orally active drugs.

Table 5
CYP-P450 Enzyme Inhibition of *L. shawii* metabolites according to SWISSADME Webserver.

Compound	CYP1A2	CYP2C19	CYP2C9	CYP2D6	CYP3A4
Costunolide	No	Yes	Yes	No	No
Catechin	No	No	No	No	No
Emodin	Yes	No	No	No	Yes
Lyciumaside	No	No	No	No	No
Aloe emodine 11-O-rhamnoside	No	No	No	No	No

confirm this, a molecular docking study was conducted using the Glide tool, and our results showed that emodin exhibited the highest docking score with two crucial amino acid interactions, including hydrogen bonding and Pi-Pi stacking with HIS94, and THR200, respectively. Moreover, multiple factors contributed to the high docking score [76] of emodin, including the type of amino acids involved in the interactions, the ligand binding pose, the type of intermolecular forces that were formed, and the distance between amino acid residues, zinc, and metabolites at the binding pocket.

To further confirm the stability of molecular docking results, a molecular dynamics simulation study was conducted for the highest docking pose of emodin. Interestingly, the protein-ligand contacts and zinc coordination were stable and consistent over the simulation run (100 ns). Additionally, our ADME and safety findings showed that most

Table 6
Organ and Endpoint Toxicity Predicted using the ProTox-II Web Server.

Compound Name	Classification				
	Organ Toxicity (% Probability)	Toxicity Endpoint (% Probability)			
	Hepatotoxicity	Carcinogenicity	Immunotoxicity	Mutagenicity	Cytotoxicity
Costunolide	Inactive (62)	Inactive (57)	Active (99)	Inactive (88)	Inactive (83)
Catechin	Inactive (72)	Inactive (51)	Inactive (96)	Inactive (55)	Inactive (84)
Emodin	Inactive (70)	Inactive (79)	Inactive (69)	Active (93)	Inactive (96)
Lyciumaside	Inactive (81)	Inactive (77)	Active (98)	Inactive (75)	Inactive (87)
Aloe emodine 11-O-rhamnoside	Inactive (84)	Inactive (74)	Active (99)	Active (63)	Inactive (85)

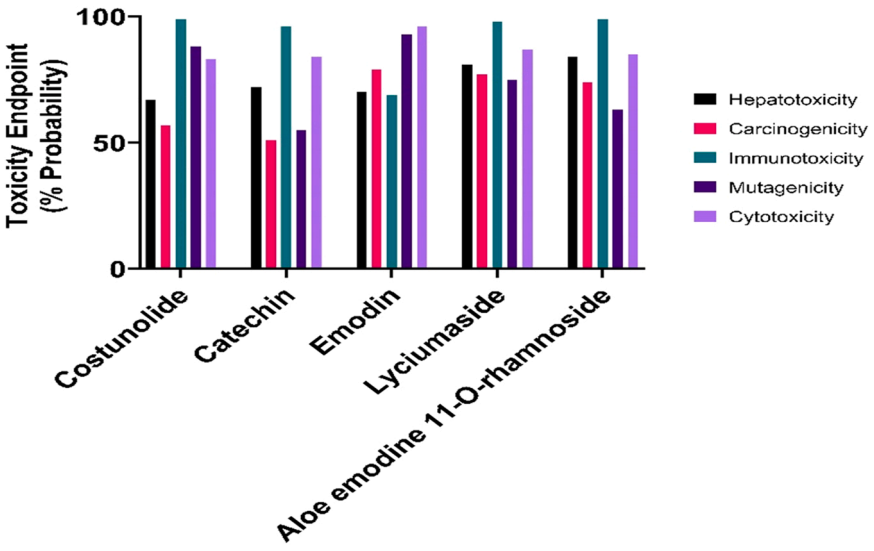

Fig. 14. The Predicted Organ and Endpoint Toxicity of L. shawii metabolites.

of the metabolites demonstrated acceptable ADME properties with no major ROF violations, minor CYP enzymes inhibition, and toxicity that could be further optimized by implementing medicinal chemistry approaches. Our study suggests that emodin could be utilized as a lead compound, optimized, and developed to generate novel CA IX inhibitors with dual therapeutic action [68]. Therefore, chemistry optimization strategies are needed to generate several analogs to improve the pharmaceutical profiles, including ADME properties and safety aspects, and perform additional *in-vitro* and *in-vivo* anti-cancer and antibacterial testing for the identified metabolites.

Taken together, our study highlights promising dual anti-cancer and anti-bacterial effects for the *L. shawii* extract *via* CA IX enzyme inhibition . The *in silico* approach appeared to predict the efficacy of green synthesized NPs successfully since it is expected to be capped with the detected *L.shawii* metabolites. Moreover, we were able to show the mechanism and the target molecule. We show the great benefit of using the *in silico* approach to search for biological drugs and recommend it in all studies.

5. Conclusion

The *L. shawii* aqueous extract was successfully used to fabricate AgNPs, and the *in vitro* tests identified the potential therapeutic efficacy of *L. shawii* metabolites and *L. shawii* -fabricated AgNPs. The antimicrobial effect of AgNPs was boosted when the NPs were conjugated with penicillin. The inhibitory effect of AgNPs against methicillin-resistant *S. aureus* and HCT116 colorectal cancer cells was strong. However, it had a weak therapeutic potential for the aggressive breast cancer cell line, MDA MBA 231. Of the *L. shawii* detected metabolites, emodin was *in silico* predicted as a promising compound for developing drugs that target the enzyme carbonic anhydrase IX. Our study highlights promising dual anti-cancer and anti-bacterial effects of the *L. shawii* extract *via* carbonic anhydrase IX enzyme inhibition, which warrants further research and investigation.

CRediT authorship contribution statement

Afrah E. Mohammed prepared the study materials and performed the *in vitro* studies and with Ishrat Rahman performed the statistical analysis. Sahar Alghamdi and Rasha Suliman performed the *in silico* study. All authors contributed to the draft preperation. Afrah E. Mohammed, Ishrat Rahman and Fuad Ameen prepared the final version and revised for submission.

Conflict of interest statement

The authors wish to declare that there is no conflict of interest.

Acknowledgment

Princess Nourah bint Abdulrahman University Researchers Supporting Project number (PNURSP2022R179), Princess Nourah bint Abdulrahman University, Riyadh, Saudi Arabia. This research was also funded by Researchers Supporting Project number (RSP-2021/364), King Saud University, Riyadh, Saudi Arabia.

Appendix A. Supporting information

Supplementary data associated with this article can be found in the online version at doi:10.1016/j.biopha.2022.113008.

References

[1] F. Moradi, S. Sedaghat, O. Moradi, S.A. Salmanabadi, Review on green nano-biosynthesis of silver nanoparticles and their biological activities: with an emphasis on medicinal plants, Inorg. Nano Metal Chem. 51 (2020) 133–142, https://doi.org/10.1080/24701556.2020.1769662.

[2] S. Ahmed, M. Ahmad, B.L. Swami, S. Ikram, A review on plants extract mediated synthesis of silver nanoparticles for antimicrobial applications: a green expertise, J. Adv. Res. 7 (2016) 17–28, https://doi.org/10.1016/J.JARE.2015.02.007.

[3] H. Chandra, P. Kumari, E. Bontempi, S. Yadav, Medicinal plants: treasure trove for green synthesis of metallic nanoparticles and their biomedical applications, Biocatal. Agric. Biotechnol. 24 (2020), 101518, https://doi.org/10.1016/J.BCAB.2020.101518.

[4] F. Ameen, P. Srinivasan, T. Selvankumar, S. Kamala-Kannan, S. al Nadhari, A. Almansob, T. Dawoud, M. Govarthanan, Phytosynthesis of silver nanoparticles using *Mangifera indica* flower extract as bioreductant and their broad-spectrum antibacterial activity, Bioorg. Chem. 88 (2019), 102970, https://doi.org/10.1016/J.BIOORG.2019.102970.

[5] P. Sathishkumar, J. Preethi, R. Vijayan, A.R. Mohd Yusoff, F. Ameen, S. Suresh, R. Balagurunathan, T. Palvannan, Anti-acne, anti-dandruff and anti-breast cancer efficacy of green synthesised silver nanoparticles using *Coriandrum sativum* leaf extract, J. Photochem. Photobiol. B Biol. 163 (2016) 69–76, https://doi.org/10.1016/J.JPHOTOBIOL.2016.08.005.

[6] N. Ahmad, S. Sharma, M.K. Alam, V.N. Singh, S.F. Shamsi, B.R. Mehta, A. Fatma, Rapid synthesis of silver nanoparticles using dried medicinal plant of basil, Colloids Surf. B Biointerfaces 81 (2010) 81–86, https://doi.org/10.1016/J.COLSURFB.2010.06.029.

[7] Z. Wang, Iron complex nanoparticles synthesized by eucalyptus leaves, ACS Sustain. Chem. Eng. 1 (2013) 1551–1554, https://doi.org/10.1021/SC400174A/ASSET/IMAGES/SC400174A.SOCIAL.JPEG_V03.

[8] N. Ramezani, Z. Ehsanfar, F. Shamsa, G. Amin, H.R. Shahverdi, H.R. Monsef Esfahani, A. Shamsaie, R.D. Bazaz, A.R. Shahverdi, Screening of medicinal plant methanol extracts for the synthesis of gold nanoparticles by their reducing

potential, Z. Naturforsch. Sect. B J. Chem. Sci. 63 (2008) 903–908, https://doi.org/10.1515/ZNB-2008-0715/MACHINEREADABLECITATION/RIS.
[9] H. Sawalha, R. Abiri, R. Sanusi, N.A. Shaharuddin, A.A.M. Noor, N.A.A. Shukor, H. Abdul-Hamid, S.A. Ahmad, Toward a better understanding of metal nanoparticles, a novel strategy from eucalyptus plants, Plants 2021 10 (2021) 929, https://doi.org/10.3390/PLANTS10050929.
[10] A. Balaji, M.V. Vellayappan, A.A. John, A.P. Subramanian, S.K. Jaganathan, M. Selvakumar, A.A. bin Mohd Faudzi, E. Supriyanto, M. Yusof, Biomaterials based nano-applications of Aloe vera and its perspective: a review, RSC Adv. 5 (2015) 86199–86213, https://doi.org/10.1039/C5RA13282G.
[11] K. Ali, S. Dwivedi, A. Azam, Q. Saquib, M.S. Al-Said, A.A. Alkhedhairy, J. Musarrat, Aloe vera extract functionalized zinc oxide nanoparticles as nanoantibiotics against multi-drug resistant clinical bacterial isolates, J. Colloid Interface Sci. 472 (2016) 145–156, https://doi.org/10.1016/J.JCIS.2016.03.021.
[12] F. Yi, L. Li, L. jia Xu, H. Meng, Y. mao Dong, H. bo Liu, P. gen Xiao, In silico approach in reveal traditional medicine plants pharmacological material basis, Chin. Med. 13 (2018) 1–20, https://doi.org/10.1186/S13020-018-0190-0/FIGURES/3.
[13] E. Ferrero, I. Dunham, P. Sanseau, In silico prediction of novel therapeutic targets using gene-disease association data, J. Transl. Med. 15 (2017) 1–16, https://doi.org/10.1186/S12967-017-1285-6/FIGURES/6.
[14] S.O. Ali Ahmad, M. Ikram, M. Imran, S. Naz, A. Ul-Hamid, A. Haider, A. Shahzadi, J. Haider, Novel prism shaped C3N4-doped Fe@Co3O4 nanocomposites and their dye degradation and bactericidal potential with molecular docking study, RSC Adv. 11 (2021) 23330–23344, https://doi.org/10.1039/D1RA03949K.
[15] M. Ikram, A. Mahmood, A. Haider, S. Naz, A. Ul-Hamid, W. Nabgan, I. Shahzadi, J. Haider, I. Ahmad, S. Ali, Dye degradation, antibacterial and in-silico analysis of Mg/cellulose-doped ZnO nanoparticles, Int. J. Biol. Macromol. 185 (2021) 153–164, https://doi.org/10.1016/J.IJBIOMAC.2021.06.101.
[16] M. Ikram, S. Hayat, M. Imran, A. Haider, S. Naz, A. Ul-Hamid, I. Shahzadi, J. Haider, A. Shahzadi, W. Nabgan, S. Ali, Novel Ag/cellulose-doped CeO2 quantum dots for efficient dye degradation and bactericidal activity with molecular docking study, Carbohydr. Polym. 269 (2021), 118346, https://doi.org/10.1016/J.CARBPOL.2021.118346.
[17] U. Qumar, J. Hassan, S. Naz, A. Haider, A. Raza, A. Ul-Hamid, J. Haider, I. Shahzadi, I. Ahmad, M. Ikram, Silver decorated 2D nanosheets of GO and MoS 2 serve as nanocatalyst for water treatment and antimicrobial applications as ascertained with molecular docking evaluation, Nanotechnology 32 (2021), https://doi.org/10.1088/1361-6528/ABE43C.
[18] M.S. Sharif, M. Aqeel, A. Haider, S. Naz, M. Ikram, A. Ul-Hamid, J. Haider, I. Aslam, A. Nazir, A.R. Butt, Photocatalytic, bactericidal and molecular docking analysis of annealed tin oxide nanostructures, Nanoscale Res. Lett. 16 (2021) 1–16, https://doi.org/10.1186/S11671-021-03495-1/FIGURES/13.
[19] S. Mureed, S. Naz, A. Haider, A. Raza, A. Ul-Hamid, J. Haider, M. Ikram, R. Ghaffar, M. Irshad, A. Ghaffar, A. Saeed, Development of multi-concentration Cu: Ag bimetallic nanoparticles as a promising bactericidal for antibiotic-resistant bacteria as evaluated with molecular docking study, Nanoscale Res. Lett. 16 (2021) 1–12, https://doi.org/10.1186/S11671-021-03547-6/FIGURES/8.
[20] M. Ikram, S. Aslam, A. Haider, S. Naz, A. Ul-Hamid, A. Shahzadi, M. Ikram, J. Haider, S.O.A. Ahmad, A.R. Butt, Doping of Mg on ZnO nanorods demonstrated improved photocatalytic degradation and antimicrobial potential with molecular docking analysis, Nanoscale Res. Lett. 16 (2021) 1–16, https://doi.org/10.1186/S11671-021-03537-8/TABLES/2.
[21] J. Hassan, S. Naz, A. Haider, A. Raza, A. Ul-Hamid, U. Qumar, J. Haider, S. Goumri-Said, M.B. Kanoun, M. Ikram, h-BN nanosheets doped with transition metals for environmental remediation; a DFT approach and molecular docking analysis, Mater. Sci. Eng.: B 272 (2021), 115365, https://doi.org/10.1016/J.MSEB.2021.115365.
[22] S.T.S. Hassan, E. Švajdlenka, Biological evaluation and molecular docking of protocatechuic acid from hibiscus sabdariffa L. as a potent urease inhibitor by an ESI-MS based method, Molecules 2017 Vol. 22 (2017) 1696, https://doi.org/10.3390/MOLECULES22101696.
[23] J. Wang, L. Tian, L. He, N. Chen, S. Ramakrishna, K.F. So, X. Mo, *Lycium barbarum* polysaccharide encapsulated poly lactic-co-glycolic acid Nanofibers: cost effective herbal medicine for potential application in peripheral nerve tissue engineering, Sci. Rep. 8 (2018) 1–14, https://doi.org/10.1038/s41598-018-26837-z.
[24] M. Thiruvengadam, B.K. Ghimire, S.H. Kim, C.Y. Yu, D.H. Oh, R. Chelliah, C. Kwon, Y.J. Kim, I.M. Chung, Assessment of mineral and phenolic profiles and their association with the antioxidant, cytotoxic effect, and antimicrobial potential of lycium chinense miller, Plants 9 (2020) 1–18, https://doi.org/10.3390/PLANTS9081023.
[25] S.S. Ali, N.A. El-Zawawy, R. Al-Tohamy, S. El-Sapagh, A.M. Mustafa, J. Sun, *Lycium shawii* Roem. & Schult.: a new bioactive antimicrobial and antioxidant agent to combat multi-drug/pan-drug resistant pathogens of wound burn infections, J. Tradit. Complement Med 10 (2019) 13–25, https://doi.org/10.1016/J.JTCME.2019.01.004.
[26] N.U. Rehman, A. Khan, A. Al-Harrasi, M. Khiat, H. Hussain, A. Wadood, M. Riaz, Natural urease inhibitors from *Aloe vera* resin and Lycium shawii and their structural-activity relationship and molecular docking study, Bioorg. Chem. 88 (2019), 102955, https://doi.org/10.1016/J.BIOORG.2019.102955.
[27] H.A. Mohammed, H.M. Ali, K.A. Qureshi, M. Alsharidah, Y.I. Kandil, R. Said, S.A. A. Mohammed, M.S. Al-Omar, O. Al Rugaie, A.A.H. Abdellatif, E. Abd-Elmoniem, M.M. Abbas, K.M. Mohany, R.A. Khan, Comparative phytochemical profile and biological activity of four major medicinal halophytes from qassim flora, Plants 2021 Vol. 10 (2021) 2208, https://doi.org/10.3390/PLANTS10102208.
[28] K.S. Siddiqi, M. Rashid, A. Rahman, A. Husen, S. Rehman, Biogenic fabrication and characterization of silver nanoparticles using aqueous-ethanolic extract of lichen (*Usnea longissima*) and their antimicrobial activity, Biomater. Res. 22 (2018) 1–9, https://doi.org/10.1186/s40824-018-0135-9.
[29] K. Chandhirasekar, A. Thendralmanikandan, P. Thangavelu, B.S. Nguyen, T. A. Nguyen, K. Sivashanmugan, A. Nareshkumar, V.H. Nguyen, Plant-extract-assisted green synthesis and its larvicidal activities of silver nanoparticles using leaf extract of *Citrus medica*, Tagetes lemmonii, and Tarenna asiatica, Mater. Lett. 287 (2021), 129265, https://doi.org/10.1016/J.MATLET.2020.129265.
[30] A. Elbermawi, A.F. Halim, E.S.S. Mansour, K.F. Ahmad, M. Elsbaey, A. Ashour, Y. Amen, M.M. El-Gamil, M. Tomofumi, K. Shimizu, Lycium schweinfurthii: new secondary metabolites and their cytotoxic activities, Nat. Prod. Res (2021) 1–8, https://doi.org/10.1080/14786419.2021.1922902.
[31] R. Mie, M.W. Samsudin, L.B. Din, A. Ahmad, N. Ibrahim, S.N.A. Adnan, Synthesis of silver nanoparticles with antibacterial activity using the lichen *Parmotrema praesorediosum*, Int. J. Nanomed. 9 (2014) 121.
[32] S. Paul, A.R.J. Singh, C.S. Sasikumar, Green synthesis of bio-silver nanoparticles by *parmelia perlata*, *ganoderma lucidum* and *phellinus igniarius* & their fields of application, Indian J. Res. Pharm. Biotechnol. 5674 (2015) 100–110.
[33] H. Arshad, M.A. Sami, S. Sadaf, U. Hassan, *Salvadora persica* mediated synthesis of silver nanoparticles and their antimicrobial efficacy, 11, Sci. Rep. 2021 11 (1) (2021) 1–11, https://doi.org/10.1038/s41598-021-85584-w.
[34] P.A. Wayne, Clinical and Laboratory Standards Institute: Performance standards for antimicrobial susceptibility testing: 20th informational supplement, CLSI Document M100-S20. (2010).
[35] A.E. Mohammed, L.A. Al-Keridis, I. Rahman, M.O. Alotaibi, R.S. Suliman, A. M. Alrajhi, M.M. Elobeid, M.R. Alothman, E.A. Alhomaidi, S.M. Korany, Silver Nanoparticles Formation by *Jatropha integerrima* and LC/MS-QTOF-Based Metabolite Profiling, Nanomaterials 11 (2021) 2400, https://doi.org/10.3390/NANO11092400.
[36] R. Ali, N. Samman, H. Al Zahrani, A. Nehdi, S. Rahman, A.L. Khan, M. Al Balwi, L. A. Alriyees, M. Alzaid, A. Al Askar, M. Boudjelal, Isolation and characterization of a new naturally immortalized human breast carcinoma cell line, KAIMRC1, BMC Cancer 17 (2017), https://doi.org/10.1186/S12885-017-3812-5.
[37] D.A. Filimonov, A.A. Lagunin, T.A. Gloriozova, A.V. Rudik, D.S. Druzhilovskii, P. V. Pogodin, V.V. Poroikov, Prediction of the biological activity spectra of organic compounds using the pass online web resource, Chem. Heterocycl. Compd. 50 (2014) 444–457, https://doi.org/10.1007/s10593-014-1496-1.
[38] D. Gfeller, A. Grosdidier, M. Wirth, A. Daina, O. Michielin, V. Zoete, SwissTargetPrediction: a web server for target prediction of bioactive small molecules, Nucleic Acids Res 42 (2014), https://doi.org/10.1093/NAR/GKU293.
[39] M.J. Keiser, B.L. Roth, B.N. Armbruster, P. Ernsberger, J.J. Irwin, B.K. Shoichet, Relating protein pharmacology by ligand chemistry, 25, Nat. Biotechnol. 2007 25 (2) (2007) 197–206, https://doi.org/10.1038/nbt1284.
[40] K.S. Watts, P. Dalal, R.B. Murphy, W. Sherman, R.A. Friesner, J.C. Shelley, ConfGen: a conformational search method for efficient generation of bioactive conformers, J. Chem. Inf. Model. 50 (2010) 534–546, https://doi.org/10.1021/CI100015J/SUPPL_FILE/CI100015J_SI_001.PDF.
[41] G. Madhavi Sastry, M. Adzhigirey, T. Day, R. Annabhimoju, W. Sherman, Protein and ligand preparation: parameters, protocols, and influence on virtual screening enrichments, J. Comput. Aided Mol. Des. 27 (2013) 221–234, https://doi.org/10.1007/S10822-013-9644-8.
[42] R.A. Friesner, R.B. Murphy, M.P. Repasky, L.L. Frye, J.R. Greenwood, T.A. Halgren, P.C. Sanschagrin, D.T. Mainz, Extra precision glide: Docking and scoring incorporating a model of hydrophobic enclosure for protein-ligand complexes, J. Med. Chem. 49 (2006) 6177–6196, https://doi.org/10.1021/JM051256O/SUPPL_FILE/JM051256OSI20060602_023733.PDF.
[43] K.J. Bowers, E. Chow, H. Xu, R.O. Dror, M.P. Eastwood, B.A. Gregersen, J.L. Klepeis, I. Kolossvary, M.A. Moraes, F.D. Sacerdoti, J.K. Salmon, Y. Shan, D.E. Shaw, Scalable algorithms for molecular dynamics simulations on commodity clusters, Proceedings of the 2006 ACM/IEEE Conference on Supercomputing. (2006) 84-es. ⟨https://doi.org/10.1145/1188455.1188544⟩.
[44] Schrodiner Release 2017–1, QikProp, (2021).
[45] N. Ur Rehman, S. Ahsan Halim, M. Khan, H. Hussain, H. Yar Khan, A. Khan, G. Abbas, K. Rafiq, A. Al-Harrasi, Antiproliferative and carbonic anhydrase ii inhibitory potential of chemical constituents from *lycium shawii* and aloe vera: evidence from in silico target fishing and in vitro testing, Pharmaceuticals 13 (2020), https://doi.org/10.3390/PH13050094.
[46] N. Ur Rehman, H. Hussain, S.A. Al-Riyami, R. Csuk, M. Khiat, G. Abbas, A. Al-Rawahi, I.R. Green, I. Ahmed, A. Al-Harrasi, Lyciumaside and lyciumate: a new diacylglycoside and sesquiterpene lactone from *lycium shawii*, Helv. Chim. Acta 99 (2016) 632–635, https://doi.org/10.1002/HLCA.201600066.
[47] J.W. De Kraker, M.C.R. Franssen, M.C.F. Dalm, A. De Groot, H.J. Bouwmeester, Biosynthesis of germacrene a carboxylic acid in chicory roots. Demonstration of a cytochrome P450 (+)-Germacrene a hydroxylase and NADP+-dependent sesquiterpenoid dehydrogenase(s) involved in sesquiterpene lactone biosynthesis, Plant Physiol. 125 (2001) 1930, https://doi.org/10.1104/PP.125.4.1930.
[48] Z. Cheng, Z. Zhang, Y. Han, J. Wang, Y. Wang, X. Chen, Y. Shao, Y. Cheng, W. Zhou, X. Lu, Z. Wu, A review on anti-cancer effect of green tea catechins, J. Funct. Foods 74 (2020), 104172, https://doi.org/10.1016/J.JFF.2020.104172.
[49] X. Dong, J. Fu, X. Yin, S. Cao, X. Li, L. Lin, J. Ni, Emodin: a review of its pharmacology, toxicity and pharmacokinetics, Phytother. Res 30 (2016) 1207–1218, https://doi.org/10.1002/PTR.5631.
[50] C. Ji, G. Xin, F. Duan, W. Huang, T. Tan, Study on the antibacterial activities of emodin derivatives against clinical drug-resistant bacterial strains and their

interaction with proteins, –92, Ann. Transl. Med. 8 (2020) 92, https://doi.org/10.21037/ATM.2019.12.100.
[51] P.H. Huang, C.Y. Huang, M.C. Chen, Y.T. Lee, C.H. Yue, H.Y. Wang, H. Lin, Emodin and aloe-emodin suppress breast cancer cell proliferation through ER α inhibition, Evid. Based Complement Altern. Med 2013 (2013), https://doi.org/10.1155/2013/376123.
[52] B. Tian, Y. Hua, Concentration-dependence of prooxidant and antioxidant effects of aloin and aloe-emodin on DNA, Food Chem. 91 (2005) 413–418, https://doi.org/10.1016/J.FOODCHEM.2004.06.018.
[53] S. Dasari, K.A. Suresh, M. Rajesh, C.S.S. Reddy, C.S. Hemalatha, R. Wudayagiri, L. Valluru, Biosynthesis, characterization, antibacterial and antioxidant activity of silver nanoparticles produced by lichens, J. Bionanosci. 7 (2013) 237–244, https://doi.org/10.1166/JBNS.2013.1140.
[54] P. Khandel, S. Kumar Shahi, L. Kanwar, R. Kumar Yadaw, D. Kumar Soni, Biochemical profiling of microbes inhibiting Silver nanoparticles using symbiotic organisms, Int. J. Nano Dimens. 9 (2018) 273–285.
[55] S. Murugesan, S. Bhuvaneswari, V. Sivamurugan, Green synthesis, characterization of silver nanoparticles of a marine red alga *spyridia fusiformis* and their antibacterial activity, Int. J. Pharm. Pharm. Sci. 9 (2017) 192–197, https://doi.org/10.22159/IJPPS.2017V9I5.17105.
[56] F. Ameen, Optimization of the synthesis of fungus-mediated Bi-metallic Ag-Cu nanoparticles, Appl. Sci. 12 (2022) 1384, https://doi.org/10.3390/APP12031384/S1.
[57] M. Chokkalingam, P. Singh, Y. Huo, V. Soshnikova, S. Ahn, J. Kang, R. Mathiyalagan, Y.J. Kim, D.C. Yang, Facile synthesis of Au and Ag nanoparticles using fruit extract of Lycium chinese and their anticancer activity, J. Drug Deliv. Sci. Technol. 49 (2019) 308–315.
[58] M.-T. Chen, W.K. Zhang, W.-L. Liang, Y.-S. Li, X.-J. Li, L.-H. Zhu, H.-B. Tang, Controllable and extra-fast synthesis of bio-applicable silver nanoparticles with *Lycium barbarum L.* aqueous extract and visible light, Mater. Technol. 34 (2019) 581–591, https://doi.org/10.1080/10667857.2019.1603656.
[59] M. Aqeel, M. Rashid, M. Ikram, A. Haider, S. Naz, J. Haider, A. Ul-Hamid, A. Shahzadi, Photocatalytic, dye degradation, and bactericidal behavior of Cu-doped ZnO nanorods and their molecular docking analysis, Dalton Trans. 49 (2020) 8314–8330, https://doi.org/10.1039/D0DT01397H.
[60] M. Ikram, J. Hassan, A. Raza, A. Haider, S. Naz, A. Ul-Hamid, J. Haider, I. Shahzadi, U. Qamar, S. Ali, Photocatalytic and bactericidal properties and molecular docking analysis of TiO_2 nanoparticles conjugated with Zr for environmental remediation, RSC Adv. 10 (2020) 30007–30024, https://doi.org/10.1039/D0RA05862A.
[61] Y. Fan, A.A. Gonzales, Enhanced antibiotic activity of ampicillin conjugated to gold nanoparticles on PEGylated rosette nanotubes, Int. J. Nanomed. (2019) 7281–7289.
[62] J.N. Payne, H.K. Waghwani, M.G. Connor, W. Hamilton, S. Tockstein, H. Moolani, F. Chavda, V. Badwaik, M.B. Lawrenz, R. Dakshinamurthy, Novel synthesis of kanamycin conjugated gold nanoparticles with potent antibacterial activity, Front. Microbiol. 7 (2016), https://doi.org/10.3389/FMICB.2016.00607.
[63] M. Shahbandeh, A. Eghdami, M. Moosazadeh Moghaddam, M. Jalali Nadoushan, A. Salimi, M. Fasihi-Ramandi, S. Mohammadi, M. Mirzaei, R. Mirnejad, Conjugation of imipenem to silver nanoparticles for enhancement of its antibacterial activity against multidrug-resistant isolates of *Pseudomonas aeruginosa*, J. Biosci. 46 (2021), https://doi.org/10.1007/s12038-021-00143-9.
[64] A. Wawruszak, M. Halasa, K. Okla, Lycium barbarum (goji berry), human breast cancer, and antioxidant profile, in: Victor R. Preedy, Vinood B. Patel (Eds.), Cancer, 2nd ed..,, Academic Press, 2021, pp. 399–406, https://doi.org/10.1016/B978-0-12-819547-5.00035-3.
[65] S.M. Monti, C.T. Supuran, G. de Simone, Carbonic anhydrase IX as a target for designing novel anticancer drugs, Curr. Med Chem. 19 (2012) 821–830, https://doi.org/10.2174/092986712799034851.
[66] J.Y. Winum, M. Rami, A. Scozzafava, J.L. Montero, C. Supuran, Carbonic anhydrase IX: a new druggable target for the design of antitumor agents, Med Res Rev. 28 (2008) 445–463, https://doi.org/10.1002/MED.20112.
[67] C.T. Supuran, Inhibition of carbonic anhydrase IX as a novel anticancer mechanism, World J. Clin. Oncol. 3 (2012) 98, https://doi.org/10.5306/WJCO.V3.I7.98.
[68] M.T.M. Nemr, A.M. AboulMagd, H.M. Hassan, A.A. Hamed, M.I.A. Hamed, M. T. Elsaadi, Design, synthesis and mechanistic study of new benzenesulfonamide derivatives as anticancer and antimicrobial agents via carbonic anhydrase IX inhibition, RSC Adv. 11 (2021) 26241–26257, https://doi.org/10.1039/D1RA05277B.
[69] N. Xu, W. Lu, L. Meng, X. Feng, J. Xuan, F. Liu, Z. Feng, Carbonic anhydrase inhibition, antioxidant activity against alveolar epithelial cells and antibacterial effect against *Klebsiella pneumoniae* enabled by synthesized silica nanoparticles through laser ablation technique, Life Sci. 278 (2021), https://doi.org/10.1016/J.LFS.2021.119032.
[70] Y. Li, H. Wang, E. Oosterwijk, C. Tu, K.T. Shiverick, D.N. Silverman, S.C. Frost, Expression and activity of carbonic anhydrase ix is associated with metabolic dysfunction in MDA-MB-231 breast cancer cells, Cancer Invest 27 (2009) 613, https://doi.org/10.1080/07357900802653464.
[71] M.J. Hsieh, K.S. Chen, H.L. Chiou, Y.S. Hsieh, Carbonic anhydrase XII promotes invasion and migration ability of MDA-MB-231 breast cancer cells through the p38 MAPK signaling pathway, Eur. J. Cell Biol. 89 (2010) 598–606, https://doi.org/10.1016/J.EJCB.2010.03.004.
[72] B. Bao, K. Groves, J. Zhang, E. Handy, P. Kennedy, G. Cuneo, C.T. Supuran, W. Yared, M. Rajopadhye, J.D. Peterson, *In vivo* imaging and quantification of carbonic anhydrase IX expression as an endogenous biomarker of tumor hypoxia, PLoS One 7 (2012), https://doi.org/10.1371/JOURNAL.PONE.0050860.
[73] E. Andreucci, J. Ruzzolini, S. Peppicelli, F. Bianchini, A. Laurenzana, F. Carta, C. T. Supuran, L. Calorini, The carbonic anhydrase IX inhibitor SLC-0111 sensitises cancer cells to conventional chemotherapy, J. Enzym. Inhib. Med Chem. 34 (2019) 117–123, https://doi.org/10.1080/14756366.2018.1532419.
[74] N.S. Abutaleb, A. Elkashif, D.P. Flaherty, M.N. Seleem, In vivo antibacterial activity of acetazolamide, Antimicrob. Agents Chemother. 65 (2021), https://doi.org/10.1128/AAC.01715-20/ASSET/2465AD23-E368-4EDF-8537-BC6141E104DF/ASSETS/IMAGES/LARGE/AAC.01715-20-F0004.JPG.
[75] S. Seršen, K. Traven, J. Kljun, I. Turel, C.T. Supuran, Organoruthenium(II) complexes of acetazolamide potently inhibit human carbonic anhydrase isoforms I, II, IX and XII, J. Enzym. Inhib. Med Chem. 34 (2019) 388–393, https://doi.org/10.1080/14756366.2018.1547288.
[76] K.K. Chaudhary, N. Mishra, A review on molecular docking: novel tool for drug discovery, a review on molecular docking: novel tool for drug discovery, JSM Chem. 4 (2016) 1029 (www.pdb.org).